Unclassified
SECURITY CLASSIFICATION OF THIS PAGE

(2)

REPORT DOCUMENTATION PAGE

1a. REPORT SECURITY CLASSIFICATION: Unclassified	1b. RESTRICTIVE MARKINGS: DTIC FILE COPY
AD-A209 998 DTIC ELECTE JUL 11 1989 D	3. DISTRIBUTION/AVAILABILITY OF REPORT: Approved for Public Release; Distribution Unlimited
	5. MONITORING ORGANIZATION REPORT NUMBER(S): AFOSR-TR-89-0519
6a. NAME OF PERFORMING ORGANIZATION: Center for Laser Studies, Univ. of Southern California	6b. OFFICE SYMBOL (If applicable):
6c. ADDRESS (City, State, and ZIP Code): University Park, DRB 17, Los Angeles, CA 90089-1112	7a. NAME OF MONITORING ORGANIZATION: Same as 8a
8a. NAME OF FUNDING/SPONSORING ORGANIZATION: AFOSR/NP	8b. OFFICE SYMBOL (If applicable): NP
8c. ADDRESS (City, State, and ZIP Code): Building 410, Bolling AFB, DC 20332-6448	7b. ADDRESS (City, State, and ZIP Code): Same as 8c
	9. PROCUREMENT INSTRUMENT IDENTIFICATION NUMBER: AFOSR-84-0378
	10. SOURCE OF FUNDING NUMBERS: PROGRAM ELEMENT NO. 61102F; PROJECT NO. 2301; TASK NO. A1; WORK UNIT ACCESSION NO.

11. TITLE (Include Security Classification)
New Efficient Optically Pumped Solid State Lasers (Unclassified)

12. PERSONAL AUTHOR(S)
Bass, Birnbaum

13a. TYPE OF REPORT	13b. TIME COVERED	14. DATE OF REPORT (Year, Month, Day)	15. PAGE COUNT
Final	FROM 8/15/84 TO 11/14/88	1989 Feb. 21	52

16. SUPPLEMENTARY NOTATION

17. COSATI CODES			18. SUBJECT TERMS (Continue on reverse if necessary and identify by block number)
FIELD	GROUP	SUB-GROUP	Solid State Lasers, Laser Spectroscopy, Ion-Ion Interactions

19. ABSTRACT (Continue on reverse if necessary and identify by block number)

This contract effort explored the effects on laser operation of ion-ion interactions in crystalline solids. Our work on the doubly-doubly Nd,Er:YAG and Nd,Ho:YAG lasers has demonstrated not only simultaneous lasing of both ionic species but also drastic lifetime reductions in the lower laser states of both Er and Ho. This work has enabled us to predict crystals in which 4 level operations at 2.9 microns can be achieved and initial verification was obtained with Er,Nd:YALO. The contract work is summarized in the published papers and PhD theses presented to the Physics and Electrical Engineering Departments of the University of Southern California.

Keywords:

20. DISTRIBUTION/AVAILABILITY OF ABSTRACT	21. ABSTRACT SECURITY CLASSIFICATION
☒ UNCLASSIFIED/UNLIMITED ☒ SAME AS RPT. ☐ DTIC USERS	Unclassified
22a. NAME OF RESPONSIBLE INDIVIDUAL: Dr. Howard Schlossberg	22b. TELEPHONE (Include Area Code): 202/767-4906
	22c. OFFICE SYMBOL: NP

DD FORM 1473, 84 MAR — 83 APR edition may be used until exhausted. All other editions are obsolete.

SECURITY CLASSIFICATION OF THIS PAGE

89 7 11 052 Unclassified

NEW, EFFICIENT OPTICALLY PUMPED SOLID STATE LASERS

Michael Bass, P.I.
Center for Laser Studies, University of Southern California
Now at University of Central Florida

Milton Birnbaum, P.I.
Center for Laser Studies, University of Southern California

FINAL REPORT

Contract No. AFOSR-84-0378
August 15, 1984 – November 14, 1988

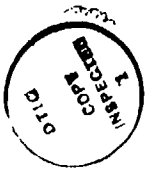

Submitted to

Air Force Office of Scientific Research
Bolling Air Force Base
Washington, DC

Attn: Dr. H. Schlossberg

INTRODUCTION

Our research work in the field of "New and Efficent Solid State Lasers", during the contract period from 15 August 1984 thru 11 November 1988 (AFOSR–88–0378) has led to some notable advances. This effort has focused on lasers in which ion–ion interactions play an important role in both the pumping and relaxation processes of the lasers. Our work on the doubly–doubled Nd,Er:YAG and Nd,Ho:YAG lasers has demonstrated not only simultaneous lasing of both ionic species but also drastic lifetime reductions in the lower laser states of both Er and Ho. This work has led to the investigation of the Nd,Er ion–ion interactions in other crystals such as Nd,Er:YALO. We have found that in this crystal the upper state (11/2) lifetime is shorter than the lower state (13/2) lifetime and thus 4–level laser operation resulting in CW laser output at 2.9 μm becomes feasible.

RESULTS AND ACCOMPLISHMENT

All of the major results of our studies have been published or are in the process of submission for publication. Therefore, our final report consists of copies of our published papers and the draft copies of those in process of publication. A list of the two PhD theses completed under this contract and two which have begun under this contract and are expected to be completed in 1989 are listed separately.

PhD theses presented: "Interactions amongst Like and Unlike Ions and Their Impact on Fluorescence Decay and Stimulated Emission Properties of Er:YAG and (Er, Nd):YAG Laser Crystals" by Weiqiang Shi, July, 1988 (Physics). and "Spectroscopic and 3 μm Lasing Properties of

Ho:$Y_3Al_5O_{12}$ Incorporating Deactivator and Sensitizer Ions" by Jason P. Machan, October, 1988. Phd Theses (Electrical Engineering) in progress: "Interactions Between dissimilar ions in (Er,Nd):$YALO_3$ by Laurie A. Fathe and "Ion – Ion Interactions and Upconversion Effects in Er,Ho:YAG" by Russell Kurtz.

The list of published papers summarizes the accomplishments under this contract. A paper in preparation is also included. Copies of these papers are given in this final report to provide a record of the work accomplished.

1. M. Birnbaum, C.L. Fincher, J. Machan and M. Bass, "Radiative Trapping Effects in Ruby: $77^{o}K$ to $300^{o}K$," JOSA B, pp. 1722–4, Dec. 1986.
2. M. Bass, W.Q. Shi, R. Kurtz, M. Kokta, and H. Diegl, "Operation of High Dopant Density Er:YAG at 2.94 μm," in Tunable Solid State Lasers II, eds. Budgor, Esterowitz and DeShazer, Springer–Verlag, N.Y., 1986 pp. 300–305.
3. M. Birnbaum, and A. Pertica, "Laser Material Characteristics of Ti^{3+}:Al_2O_3." JOSA B, pp. 1434–6, Sep. 1987.
4. M. Birnbaum, "Fluorescence of Large Ruby Laser Rods," Applied Spectroscopy, pp. 1448–9, vol. 41, Number 8, 1987.
5. W.Q. Shi, R. Kurtz, J. Machan, M. Bass, M. Birnbaum and M. Kokta, "Simultaneous, Multiple Wavelength Lasing of (Er, Nd): $Y_3Al_5O_{12}$," Applied Physics Letters, Oct. 19, 1987 pp. 1218–20.
6. J. Machan, R. Kurtz, M. Bass, M. Birnbaum, and M. Kokta, "Simultaneous, Multiple Wavelength Lasing of (Ho,Nd):$Y_3Al_5O_{12}$," Applied Physics Letters, Oct. 26, 1987,

pp. 1313–15.

7. W.Q. Shi, M. Bass and M. Birnbaum, "Investigation of the Interactions Between Dissimilar Ions in (Er, Nd):$Y_3Al_5O_{12}$," JOSA B, pp. 23–29, January 1989.

Paper in process of publication:

8. W.Q. Shi, M. Bass, and M. Birnbaum, "Effects of Energy Transfer Amongst Er^{3+} Ions on the Fluorescence Decay and Lasing Properties of Heavily Doped Er:$Y_3Al_5O_{12}$".

Reprinted from Journal of the Optical Society of America B, Vol. 3, page 1722, December 1986

Radiative trapping effects in ruby: 77 to 300 K

Milton Birnbaum and Curtis L. Fincher

The Aerospace Corporation, P.O. Box 92957, Los Angeles, California 90009

Jason Machan and Michael Bass

Center for Laser Studies, Los Angeles, California 90007

Received July 22, 1986; accepted September 8, 1986

The fluorescent decay of the ^2E level of Cr^{3+} over the range of 77 to 300 K has been studied in experimental arrangements providing strong trapping of the *O*-phonon lines. At 300 K, rubies as large as 2.5-cm diameter by 33-cm length were used and were packed in highly reflective $BaSO_4$ powder to provide adequate trapping of the *O*-phonon fluorescence. The measurements resulted in the determination explicitly of the lifetime vibronic transitions and the *O*-phonon decay rate. These studies of lifetime enhancement have potential application in the design of efficient solid-state lasers.

INTRODUCTION

Radiative trapping effects are important in the operation of lasers. A well-known example is the Cu-vapor laser,[1] in which radiative trapping of the pump radiation is utilized to increase the lifetime of the pumped level and thereby to alleviate the stringent requirements on the rise time and duration of the pump pulse. In general, radiative trapping effects in solids are less pronounced than in gases because of the difficulty of meeting the requirement that the emitted fluorescence be resonantly reabsorbed. In ruby, Nelson and Sturge[2] showed that self-absorption of the fluorescence (radiative trapping) could be used to obtain the lifetime of the vibronic transitions for the ^2E upper level. We have extended their results and have obtained the lifetime associated with the vibronic transitions at 77 and 300 K and explicitly the lifetimes of the *O*-phonon transitions.

THEORETICAL CONSIDERATIONS

The spectroscopy of the *R*-line fluorescence in ruby has been extensively studied,[2] stimulated by the utility of ruby as a laser material (in fact, it was the material of the first laser). The relevant aspects of the energy-level diagram and the fluorescence emissions are shown, respectively, in Figs. 1 and 2. The R_1 and R_2-line emissions are *O*-phonon lines,[2] and strong reabsorption (trapping) can be readily obtained.

An estimate of the magnitude of the radiative trapping effect was obtained from the analysis of Holstein.[3] For a Gaussian line with a peak absorption coefficient of α_m, Holstein finds that in a long cylinder of radius R the lifetime is lengthened by the factor

$$\tau_{tr}/\tau_{utr} = 0.63\alpha_m R[\ln(\pi\alpha_m R/2)]^{1/2}, \qquad (1)$$

where τ_{tr} is the trapped or lengthened lifetime and τ_{utr} is the untrapped lifetime. In a ruby crystal of practical dimensions (1.60-cm diameter by 19-cm length) Eq. (1) predicts that an opaquely silvered rod will show a large lifetime-lengthening factor (practically complete trapping of the *O*-phonon lines of ruby at 77 K).

The observed lifetime, τ_{obs}, of the red-line fluorescence is given by

$$1/\tau_{obs} = 1/\tau_1 + 1/\tau_2 + 1/\tau_3, \qquad (2)$$

where τ_1 is the lifetime of *O*-phonon lines, τ_2 the lifetime of the vibronic lines, and τ_3 the nonradiative lifetime of the fluorescing levels. For the case of strong trapping, $\tau_1 \gg \tau_3$, τ_2 and $1/\tau_{obs} \simeq 1/\tau_2 + 1/\tau_3$. From spectroscopic studies, τ_3 can be estimated, thereby leading to a determination of the lifetimes of the vibronic lines, τ_2. At 77 K, the lifetime τ_2 of the vibronic lines is much shorter than that of the nonradiative lifetime τ_3, leading to the expression $1/\tau_{obs} \simeq 1/\tau_2$ and to a direct measurement of τ_2.

EXPERIMENTAL METHOD

A cold-finger arrangement was utilized for measurements of the smaller rubies (see Table 1) over the temperature range of 77 to 300 K. The larger rubies (Table 1) were studied at 300 K only.[4] All samples in this work had Cr^{+3} concentrations of ~0.05%. At 77 K, data were obtained with bare ruby rods and opaquely silvered ruby rods with small apertures to introduce the pumping radiation and to permit the exit of the fluorescence. The fluorescence was excited by chopping the output of a Spectra-Physics cw Ar-ion laser operating at 514.5 nm to produce pulses of duration short in comparison with the fluorescent lifetimes. The large ruby rods (2 cm × 25 cm and 2.5 cm × 33 cm) were measured at room temperature only. They were packed tightly in a $BaSO_4$ powder, which provided a diffuse reflectivity greater than 99.5%.[5] For these rods, the excitation-light input port and the observation ports were thin optical fibers attached with an optical cement at several positions along the rod's cylindrical surface.

A typical example of the computer-processed data is shown in Fig. 3, in which the averaged fluorescence data of 100 pulsed excitations are shown. In general, the precision of a lifetime measurement was about 4%. The fluorescence-lifetime measurements of rods 5 and 6 were taken at exit ports near the excitation port and at the most distant ports.

0740-3224/86/121722-03$02.00

K. This result is expected since at room temperature there is a small but appreciable population in the $^2T_1$ level, ~500 cm^{-1} above the metastable ^2E level. The radiative decay of the $^2T_1$ is much faster than that of the ^2E level, and this could account for the reduced lifetimes at room temperature.

The values of columns 5 and 6 of Table 1 were obtained with the aid of Eq. (3):

$$1/\tau_{utr} = 1/\tau_1 + 1/\tau_2 + 1/\tau_3, \quad (3)$$

where τ_{utr} is the untrapped lifetime and τ_3 is the lifetime of the nonradiative transitions. The values of τ_{utr} are 4.3 and 3.3 msec at 77 and 300 K, respectively.[2] At 77 K, τ_3 is much greater than τ_1 and τ_2 and can be neglected in Eq. (3), whereas at 300 K, $\tau_3 \approx 20$ msec.[2] At 77 K, $1/\tau_{obs} = 1/\tau_2$ since $\tau_1 \gg \tau_2$. Therefore $\tau_2 = \tau_{obs}$ for the first four rows of Table 1. To obtain τ_1, we note that $1/\tau_{utr} = 1/\tau_1 + 1/\tau_2$ or $1/\tau_1 = 1/\tau_{utr} - 1/\tau_{obs}$. The results listed in Table 1 for the large rubies at 300 K can be obtained similarly: $1/\tau_1 = 1/\tau_{utr} - 1/\tau_{obs}$, and therefore $1/\tau_2 = 1/\tau_{obs} - 1/\tau_3$.

CONCLUSIONS

The fluorescent decay of the ^2E level of the Cr^{3+} over the range of 77 to 300 K has been studied in experimental arrangements providing strong trapping of the O-phonon lines. This has resulted in the determination explicitly of the lifetime of the vibronic transitions, τ_2, and the O-phonon decay rate, τ_1.

ACKNOWLEDGMENT

The support of the U.S. Air Force Office of Scientific Research under AFOSR grant no. AFOSR-84-0378 is acknowledged.

REFERENCES AND NOTES

1. L. A. Weaver, C. S. Liu, and E. W. Sucov, "Superradiant emission at 5106, 5700, and 5782 Å in pulsed copper iodide discharges," IEEE J. Quantum Electron. QE-10, 140–1XX (1974).
2. D. F. Nelson and M. D. Sturge, "Relation between absorption and emission in the region of the R-lines of ruby," Phys. Rev. 137, A1117–A1130 (1965).
3. T. Holstein, "Imprisonment of resonant radiation in gases," Phys. Rev. 172, 1212–1233 (1947).
4. Loaned to us by John McMahan, Optical Physics Division, Naval Research Laboratory, Washington, D.C.
5. We acknowledge participation in these experiments by Jackson Jung, a Summer High School Fellow at the University of Southern California.

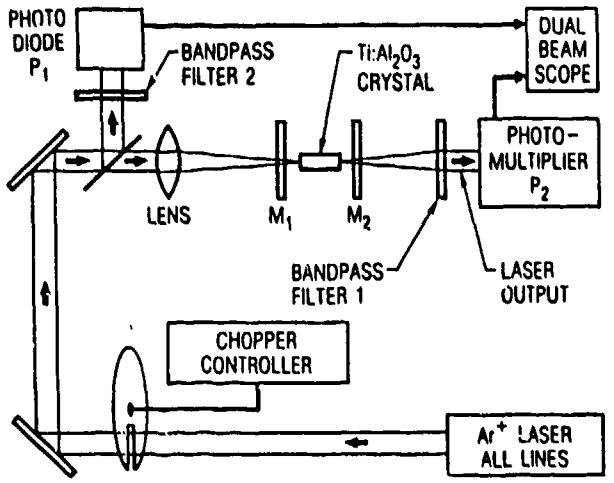

Fig. 1. Block diagram of the experimental arrangement. M_1, M_2, mirrors.

EXPERIMENTAL RESULTS

The emission spectra of the $Ti:Al_2O_3$ lasers are pump-power dependent. In Fig. 2, the typical output band as a function of pump power is shown. Near threshold the laser output is restricted to a narrow band of about 7 nm centered close to 780 nm. The emission cross sections and loss coefficients refer specifically to this wavelength band. However, by normalizing the emission cross section to the relative fluorescence intensity as a function of wavelength, the stimulated emission cross sections can be estimated over the entire band.[8] A similar procedure could be followed for the loss coefficients by normalizing to the absorption spectrum of the residual losses.[3] However, since this is not precisely known and probably varies with the crystal specimen, only a rough estimate can be gained by this procedure.

In Fig. 2, we note that the output power does not increase linearly with increasing pump power. This was attributed to heating of the Ti:sapphire sample at the higher pump level that reduces the fluorescence lifetime (approximately 3.2 μsec at 300 K) and raises the required threshold pump power.

Threshold measurements are reported for samples numbers 1 and 3. Samples 1 and 3 were grown by using the Czochralski technique.[5] A heavily doped Czochralski sample was also studied. The high losses precluded quasi-cw operation for this sample, and, consequently, measurements for this sample are not reported.

The absorbed power was calculated from the incident power by using the following formula;

$$P_{ABS} = P_{INC} \times T_{LENS} \times T_{MIRROR} \times T_{SURFACE} \times A_{BULK}. \quad (2)$$

The incident power (P_{INC}), transmission of the front mirror, the lens, and the front crystal surface, all at the pump wavelength, and the bulk absorption of the crystal were all measured.

For crystals 1 and 3 the measurements of power absorbed at threshold versus output mirror reflectivity are shown in Fig. 3. From the y intercepts of the lines, the losses per centimeter were obtained and are shown in Fig. 3; they are 0.03 ± 0.01 (rod number 1) and 0.04 ± 0.01 (rod number 3).

In order to obtain the cross-section values from the slope of the lines Eq. (3) was utilized[6]:

$$\sigma = M \frac{h\nu_p \pi d^2}{8\eta_p \tau}, \quad (3)$$

where M is the slope of the lines in Fig. 3 and the other symbols are defined above. Typical performance data are shown in Fig. 3.

The diameter of the pumped filament was measured, using the scanning-blade–beam-scan technique, to be 102 μm. The quantum efficiency of Ti:sapphire was taken to be 75%, consistent with reported values.[2,3] A value of 500 nm was chosen as the average pump wavelength since the argon-ion pump laser emits at 488 and 514 nm. Using the above values, the average σ was found to be $2.6 \pm 0.8 \times 10^{-19}$ cm^2. This value is in reasonable agreement with the published values.[8]

A novel feature of this study was the determination of the

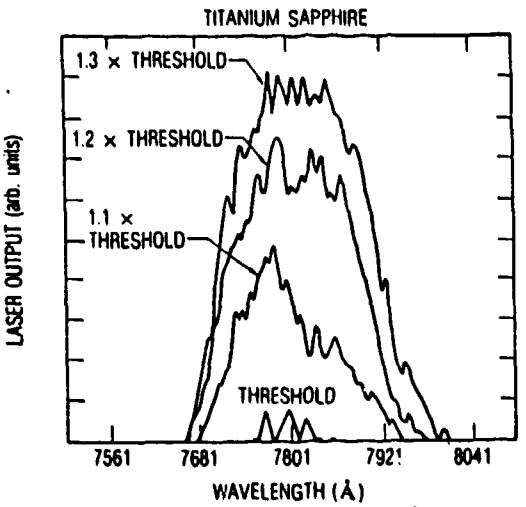

Fig. 2. Laser output spectrum of rod number 1 (R_1 = 99.9%, R_2 = 98.0%) as a function of pump power.

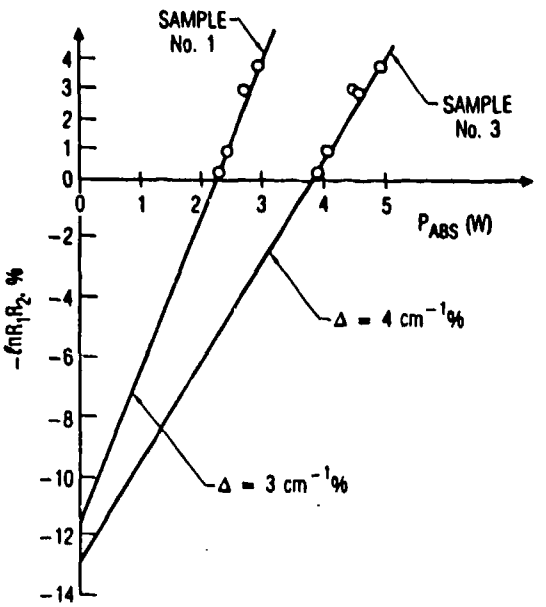

Fig. 3. Output mirror reflectivity versus power absorbed at threshold for $Ti:Al_2O_3$ rods numbers 1 and 3.

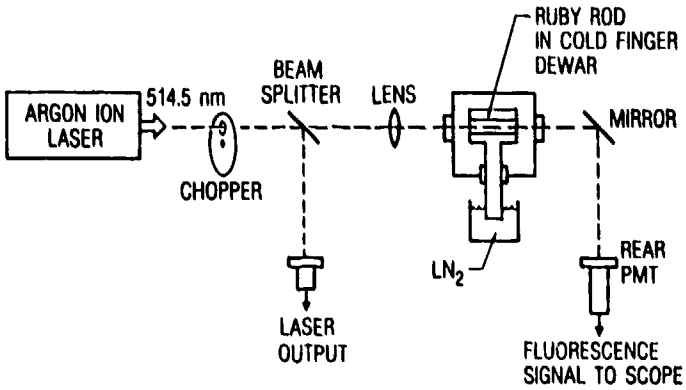

FIG. 1. Experimental arrangement for fluorescence lifetime measurements, 77 K to 300 K.

Fluorescence of Ruby Laser Rods

MILTON BIRNBAUM

Center for Laser Studies, University of Southern California, Los Angeles, California 90089

Index Headings: Luminescence.

INTRODUCTION

Fluorescence studies of the R-line emission of ruby laser rods over the temperature range of 77 to 300 K have disclosed several new features. In particular, for most of the ruby rods, the fluorescent decay time, τ, was not strictly exponential. Effects of this kind have been observed in the fluorescent decay of the $^4F_{3/2}$ level of Nd^{3+} in YAG[1] (yttrium aluminum garnet) and in Nd-doped glasses.[2] In both cases, the nonexponential decay was interpreted as evidence for inhomogeneous line broadening effects, among which are strains, ion clustering, and other defects that modify the crystal field at the ion site. Our observations of nonexponential fluorescent decay in ruby are indicative of inhomogeneous line broadening effects in lightly doped (0/05%) ruby. In fact, inhomogeneous line broadening was observed in ruby at liquid helium temperatures, in the spectroscopic studies of A. L. Schawlow.[3]

EXPERIMENTAL METHOD

The experimental arrangement which was used throughout these experiments is shown in Fig. 1 and is similar to that used by Birnbaum *et al.*[4] A cw argon-ion laser (5145 Å) was used to excite the fluorescence. In order that pulses of a few ms duration could be obtained, a chopper was inserted in the output beam of the laser. The fluorescent decay times were measured by photographing of the fluorescence decay displayed on a Tektronix oscilloscope.

Narrow bandpass filters at 694 nm and neutral-density filters were positioned in front of the photomultiplier

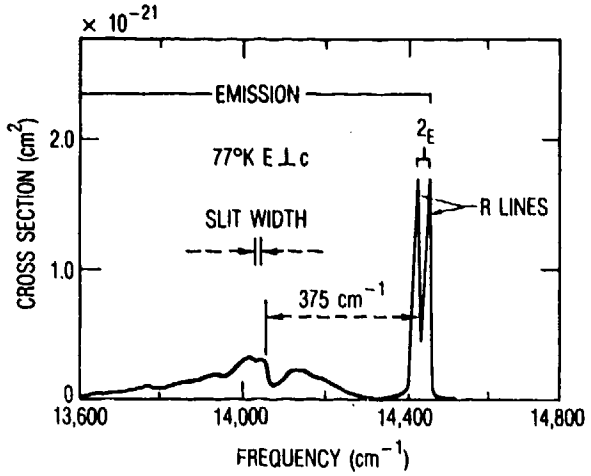

FIG. 2 Emission spectrum of dilute ruby in the vicinity of the R lines at 77 K.

Received 18 May 1987.

0003-7028/87/4108-1448$2.00/0

TABLE I. Fluorescent lifetime of ruby rods: 77 K.[a]

Ruby rod	Diam. × length (cm)	Lifetime, τ (ms) $t_1 = 7.5$ ms	$t_2 = 16.5$ ms	$t_3 = 32.5$ ms	$t_4 = 48.5$ ms
1	0.64 × 0.32	11.2	11.4	11.6	
2	0.64 × 2.5	13.8	14.4	14.6	
3	0.64 × 3.9	16.6	16.8	16.4	
4	0.64 × 5.1	14.4	15.0	15.3	
5	0.95 × 2.9	12.8	14.7	15.4	
6	1.1 × 5.3	13.2	15.5	17.0	16.6

[a] t_1, t_2, t_3, t_4 = delay after the excitation pulse for the determination of τ.

TABLE II. Fluorescent lifetime of ruby rods: 300 K.

Ruby rod	Diam. × length (cm)	Lifetime, τ (ms) $t_1 = 7.5$ ms	$t_2 = 16.5$ ms	$t_3 = 32.5$ ms
1	0.64 × 0.32	3.9	3.9	
2	0.64 × 2.5	3.8	4.4	
3	0.64 × 3.9	5.5	5.8	
4	0.64 × 5.1	4.1	4.5	4.7
5	0.95 × 2.9	3.9	4.6	4.5
6	1.1 × 5.3	4.0	5.4	5.8

tube (PMT). Thus, only red fluorescent photons were recorded, and the PMT functioned in the linear range. Data were obtained both with the lens in and with the lens removed. A copper cold finger, which surrounded the rods (except for the end faces), was used to cool the rods to ~77 K.

The fluorescence spectrum of ruby (transitions from the ^2E metastable level) is shown in Fig. 2. The long wavelength emission (peaking at 375 cm^{-1} from the R-lines) results from transitions to the vibronic sidebands of the ground state. The narrow band filters in front of the PMT permitted detection of only the R-line emissions.

EXPERIMENTAL RESULTS

Tables I and II summarize the experimental results for the ruby rods (numbers 1 to 6), which were of 90% orientation and had plane parallel polished end faces and polished cylindrical barrels. All were grown by the Czochralski method. The measured lifetimes (precision of ±7%) are listed as a function of the delay (t) in the start of the lifetime measurement following the excitation pulse of the argon-ion laser (Fig. 1). The precision of these measurements (±7%) was obtained by comparison of the oscilloscope technique measurements with those of the more precise computerized data acquisition system.[4] The increase in lifetime, τ, with t is clearly in evidence in Table I for rubies 5 and 6. A smaller increase with t is noted for rubies 1, 2, and 4, while for ruby 3, τ is essentially constant.

At 77 K, measurement of the ^2E Cr^{3+} lifetime, using very small samples to minimize effects of radiative trapping, yielded a value of 4.3 ms.[4] The τ values for rubies 3 to 6 at a delay (t_3) of 32.5 ms corresponded to the values obtained for essentially completely trapped R-line fluorescence.[4] In Ref. 4, we showed that, at 77 K, a fluorescence lifetime of about 16 ms represents the untrapped fluorescence, τ, to the phonon-terminated transitions. The nonexponential decay is attributed to the inhomogeneous line broadening processes present in the ruby rods.[3] With the use of this interpretation, the ruby rods can be ranked approximately in the order of increasing inhomogenous linewidth as follows: rod 3; rods 1, 2, and 4; and rods 5 and 6. This ranking implies that rod 3 is of the highest quality, at least in regard to the smallest inhomogeneous line broadening.

The results at 300 K, summarized in Table II, are similar to those of Table I. However, the increase in lifetime, τ, with measurement delay, t, is not as pronounced. At 300 K, the fluorescence linewidth is dominated by homogeneous broadening effects which mask the inhomogeneous linewidth. Only rod 6 shows a pronounced increase in τ with t, with smaller increases noted for rods 4 and 5. It is evident that if the nonexponential fluorescent decay is to be used to obtain information about the crystal field site inhomogeneities, one requires low temperatures to observe the inhomogeneous line broadening effects.

CONCLUSIONS

Nonexponential fluorescent decay of the ^2E level of Cr^{3+} in Al_2O_3 was observed in several ruby laser rods. This effect can be attributed to the crystal field inhomogeneity at the Cr^{3+} sites. The measurement of fluorescent decay of relevant levels in crystals can provide a simple means of observing inhomogeneous line broadening effects. The method should be generally applicable to a wide variety of laser crystals.

ACKNOWLEDGMENT

The excellent support of Curtis L. Fincher throughout the experimental investigations is gratefully acknowledged.

1. K. K. Deb, R. G. Buser, and J. Paul, Appl. Opt. **20**, 1203 (1981).
2. S. E. Stokowski, "Glass Lasers," in *Handbook of Laser Science and Technology*, M. J. Weber, Ed. (CRC Press, Boca Raton, Florida, 1982), Vol. 1, pp. 248–256.
3. A. L. Schawlow, in *Advances in Quantum Electronics*, J. R. Singer, Ed. (Columbia Univ. Press, New York, 1961), p. 52.
4. M. Birnbaum, C. L. Fincher, J. Machan, and M. Bass, Jour. Opt. Soc. Amer. B **3**, 1722 (1986).

Operation of the High Dopant Density Er:YAG at 2.94 μm

M. Bass[1], *W.Q. Shi*[1], *R. Kurtz*[1], *M. Kokta*[2], and *H. Diegl*[3]

[1]Center for Laser Studies, University of Southern California, Los Angeles, CA 90089, USA
[2]Union Carbide Corporation, Washougal, WA 98671, USA
[3]Allied Corporation, Westlake Village, CA, USA

1. Introduction

Free-running, pulsed, flashlamp-excited operation of 50 and 33% Er doped YAG lasers is reported at 2.94 μm. This laser was described by researchers in the Soviet Union as early as 1975.[1] Since then there have been a number of further reports concerning this material all published by Soviet scientists. This paper represents, to our knowledge, the first publication outside of the Soviet Union about high dopant density Er:YAG laser operation. In addition to confirming some of the performance properties described earlier, this paper presents the unusual temporal waveforms of the Er:YAG, 2.94 μm laser. An outline is given of possible pumping and relaxation processes which may contribute to the laser's operation.

Er:YAG does not lase well at 2.94 μm when the concentration of Er is the usual 1%. However, when larger concentrations are used (generally over 15%) operation at this wavelength can be quite efficient. The relevant spectroscopic data for lasing at this wavelength are given below for 50% Er:YAG:

Upper laser level	$^4I_{11/2}$
Lower laser level	$^4I_{13/2}$
Upper level lifetime	100 μsec
Lower level lifetime	2 msec
Emission cross-section	2.6×10^{-20} cm^2
Pump absorption bands	0.80 μm ($^4I_{15/2}$ - $^4I_{9/2}$)
	0.65 μm ($^4I_{15/2}$ - $^4F_{9/2}$)
	0.54 μm ($^4I_{15/2}$ - $^4S_{3/2}$)
	0.52 μm ($^4I_{15/2}$ - $^2H_{11/2}$)
	0.49 μm ($^4I_{15/2}$ - $^4F_{7/2}$)
	0.45 μm ($^4I_{15/2}$ - $^4F_{5/2}$)
	0.44 μm ($^4I_{15/2}$ - $^4F_{3/2}$)
	0.41 μm ($^4I_{15/2}$ - $^2H_{9/2}$)
	0.38 μm ($^4I_{15/2}$ - $^4G_{11/2}$)

2. Laser Tests

The laser tests were conducted in a water-cooled, double elliptical pump cavity. This cavity had been designed for pumping Alexandrite laser rods and so had the desired silver-backed pyrex reflector. While the laser may work in a gold-plated cavity, the many visible, blue and near uv pump bands suggest better efficiency is possible with a silver pump reflector. The rods reported in this paper were 6.25 mm in diameter and 120 mm long. They were obtained from Union Carbide Corp. and Crystal Optics Research Inc. The flashlamps were 6.5 mm bore diameter, xenon-filled lamps from ILC and, in the pump cavity used, were able to pump 96.5 mm of the rod. Two different pump pulse durations were used; one, called the short pump pulse, was 120 μsec long at full width at half maximum (FWHM) and the other, called the long pump pulse, was 170 μsec FWHM. The resonators mirrors were spaced only 25 cm apart to provide a resonator that was relatively insensitive to thermal lensing in the laser rod. The 100% reflector used was an uncoated, polished copper mirror with a 5 m radius of curvature. Several flat output mirrors were tested but best performance was observed for all rods with a 75% reflector. All tests were conducted with no intracavity apertures and so represent long pulse, multimode lasing in which the whole rod aperture was filled with many oscillating modes.

The performance of the Er:YAG lasers tested is summarized in Figs. 1 and 2. Fig 1 a compares the performance of the 33% doped rod when pumped with the two different pump pulses mentioned above. The

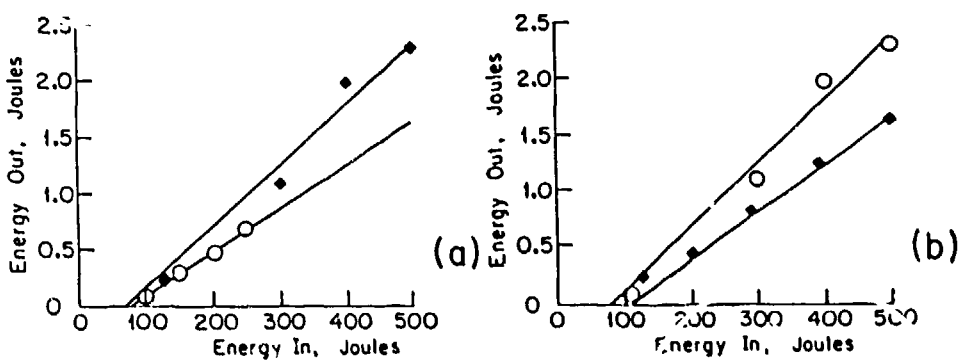

Fig. 1 A. Long pulse laser output energy of 33% doped Er:YAG at 2.94 μm versus input energy. Pump pulse duration =120 μsec for o and 170 μsec for ♦.

B. Long pulse laser output energy versus input energy for two different Er dopant densities in YAG. o = 33% and ◇ = 50%.

improvement in efficiency as the pump pulse duration is increased agrees with observations reported previously[2] and suggests that the reported 3-5% efficiencies are realizable. Fig. 1b shows the relative performance of the 33 and 50% doped rods. when pumped with the long pump pulse. The difference observed may be specific to the pump pulse waveform and pump cavity used in this work. The performance differences may depend on these parameters and so this data should not be taken as a firm preference for the 33% rod over the 50% rod. More research is necessary with excitation conditions properly tailored to the rod to be used. Both rods showed excellent optical quality when observed through crossed polarizers and no significant scattering of a HeNe beam could be detected. It should be noted that the 0.63 μm HeNe beam is attenuated in Er:YAG but the orange HeNe line is transmitted and should be used.

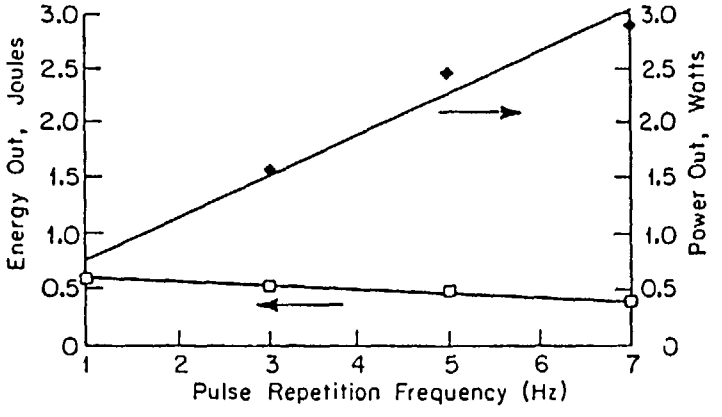

Fig. 2 Energy and power output of the 33% Er:YAG versus pump repetition rate using the 120 μsec duration pump pulse.

Fig. 2 shows the average power obtained using the 33% rod and the short pump pulse. These tests were limited by power supply considerations and it is clear that much higher average powers are possible. When the long pump pulse was used the maximum power supply repetition frequency was 3 Hz. At this prf over 5 W of average power was observed. The drop-off in energy per pulse indicates the onset of thermal lensing in the medium. Since no corrective measures were taken other than using a short resonator this problem can benefit from further laser engineering.

A major design consideration in developing this laser is preparing reliable, damage-resistant optical coatings. The major coating

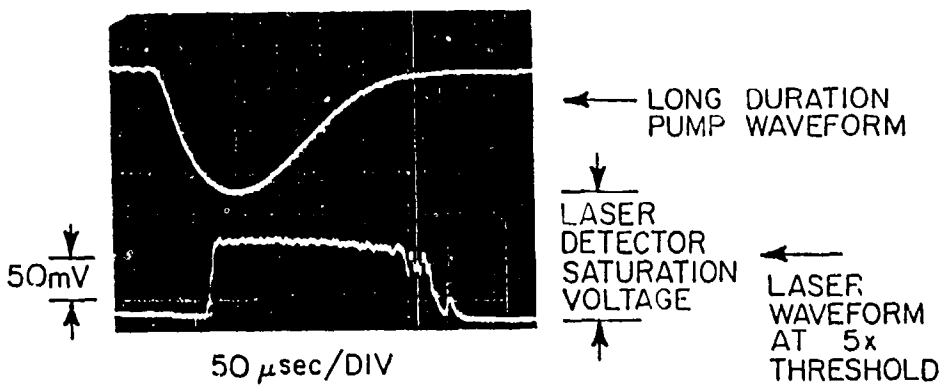

Fig. 4 Er:YAG laser waveform at 5 times threshold.

continuously without RO spikes typical of optically pumped solid state lasers. This type of RO spike does not appear until the pump has fallen well below threshold. It is expected that the improved performance reported for longer pump pulses is related to this mode of lasing in which some process operates to alter and extend the population inversion.

3. Discussion

The long pulse performance of the Er:YAG laser in terms of both energy per pulse and average power has been shown to be comparable to other optically pumped solid-state lasers. Higher outputs and efficiencies can be expected using longer duration pump pulses.[3]

The unusual waveforms observed at high output energies are the result of a combination of processes. These include contributions to the inversion due to:

1, the usual "four-level" pumping process involving excitation from the $^4I_{15/2}$ ground state,

2, "three-level" pumping from the long-lived lower laser level, the $^4I_{13/2}$ state, and

3, cross-relaxation between nearby Er^{3+} ions. The cross-relaxation process is one in which an ion in the $^4I_{13/2}$ state relaxes to the $^4I_{15/2}$ state while, simultaneously, a neighboring ion in the $^4I_{13/2}$ jumps to the $^4I_{9/2}$ state.

When in the $^4I_{9/2}$ state the ion rapidly relaxes into the upper laser level. The process of cross-relaxation is particularly important in high concentration material and is discussed in detail by Bagdasarov

et al.[4] An analysis is in progress of the relative importance of the several processes of excitation and relaxation as they contribute to the observed quasi-continuous lasing. This work will be reported at a later date.

The 2.94 μm operation of the Er:YAG laser is sufficiently interesting to warrant further study. It is a material which can be grown easily and lases well. It has potential application in surgery and as a source to drive a variety of infrared sources at important wavelengths. Since it is compatible with existing Nd:YAG laser systems exploration of its potential is straightforward. As has been pointed out in the present work and in the work of the Soviet scientists, optimum efficiency requires longer duration pump sources and so conversion of Nd:Glass or ruby lasers may lead to better performance. Reliable optical coatings for 2.94 μm requires that they be specified to contain and adsorb no water. As a result of this work it is clear that the Er:YAG laser is available to anyone who wishes to use it.

Acknowledgment

The work at U.S.C. was supported by AFOSR Contract No. AFOSR-84-0378.

References

[1]E. V. Zharikov, V. I. Zhekov, L. A. Kulevskii, T. M. Murina, V. V. Osiko, A. M. Prokhorov, A. D. Savel'ev, V. V. Smirnov, B. P. Starikov, and M. I. Timoshenko, Sov. J. of Quantum Electronics 4, 1039 (1975)

[2] V. I. Zhekov, V. A. Lobachev, T. M. Murina and A. M. Prokhorov, Sov. J. Quantum Electron. 13, 1235 (1984)

[3]I. A. Scherbakov, General Physics Institute, Moscow, USSR, seminar presented at U.S.C., June 1986

[4] Kh. S. Bagdasarov, V. I. Zhekov, V. A. Lobachev, A. A. Manenkov, T. M. Murina and A. M. Prokhorov, Izvestiya Akademii Nauk SSSR, 48, 1765, (1984)

Simultaneous, multiple wavelength lasing of (Er, Nd):$Y_3Al_5O_{12}$

W. Q. Shi, R. Kurtz,[a] J. Machan, M. Bass, and M. Birnbaum
Center for Laser Studies, University of Southern California, Los Angeles, California 90089-1112

M. Kokta
Union Carbide Corporation, Washougal, Washington 98671

(Received 8 June 1987; accepted for publication 7 August 1987)

Simultaneous lasing of both Er^{3+} and Nd^{3+} ions in yttrium aluminum garnet is reported. The crystal was doped with 15% Er^{3+} and 1% Nd^{3+}. The Er^{3+} ions lased at 2.94 μm and the Nd^{3+} ions in a broadband from 1.01 to 1.15 μm with a strong peak at 1.064 μm. Significant ion-ion interaction is suggested by the drastically altered fluorescent lifetimes and unusual lasing properties.

The erbium:yttrium aluminum garnet (Er:YAG) laser has been reported as an efficient 2.94-μm source when high concentrations (>10%) of Er^{3+} are used.[1] This lasing involves a transition from the $^4I_{11/2}$ to the $^4I_{13/2}$ state. Since the $^4I_{13/2}$ is a long-lived state compared to the $^4I_{11/2}$, lasing involving such a transition should be self-terminated. However, the $^4I_{13/2}$ state can cross relax in such a manner as to enable efficient lasing.[2] Cross relaxation of the $^4I_{13/2}$ level of Er^{3+} involves the simultaneous decay of one ion from this level to the $^4I_{15/2}$ ground state and excitation of a second ion from the $^4I_{13/2}$ to the $^4I_{9/2}$. Due to the energies associated with these states the total energy stored in the system of two ions is conserved by such a pair of transitions. The ion in the $^4I_{9/2}$ state relaxes rapidly to the $^4I_{11/2}$ state and so the net change in the population difference due to cross relaxation is 3. Such a cross relaxation process actually increases the population difference and enables the phenomenon of quasicontinuous lasing.[3] An approach to improving the 2.94-μm lasing of Er^{3+} was suggested by Kaminskii *et al.*[4] They pointed out that Nd^{3+} ions in the Er:YAG crystal could cross relax the Er^{3+} $^4I_{13/2}$ state and, perhaps, reduce the problem of self-termination. We have followed this suggestion and report, for the first time to our knowledge, on the multiwavelength lasing properties of YAG doped with 15% Er^{3+} and 1% Nd^{3+} ions. Simultaneous lasing was observed at 2.94 μm by the Er^{3+} ions and in a band from 1.01 to 1.15 μm presumably by the Nd^{3+} ions. There is a strong peak at 1.06 μm in the band of emitted laser light.

An examination of the energy levels of Er^{3+} and Nd^{3+} ions in YAG reveals that the Er^{3+} $^4I_{13/2}$ and the Nd^{3+} $^4I_{15/2}$ levels are nearly isoenergetic.[5] This observation led to the suggestion made by Kaminskii *et al.* that the Er^{3+} ions could be cross relaxed by the Nd^{3+} ions.[4] Furthermore, since the Nd^{3+} $^4I_{15/2}$ level is known to relax very rapidly to the $^4I_{9/2}$ ground state this cross relaxation could provide a rapid and efficient means of reducing or eliminating the self-termination of the 2.94-μm Er^{3+} transition. Measurements of various Er^{3+} state lifetimes in 16.7% Er:YAG and in (15% Er, 1% Nd):YAG and of the Nd^{3+} $^4F_{3/2}$ state lifetime in 1% Nd:YAG and (15% Er, 1% Nd):YAG were made and are listed in Table I. It is clear from these results that the introduction of Nd^{3+} strongly affects the Er^{3+} and vice versa.

The entry in Table I for the Nd^{3+} $^4F_{3/2}$ state lifetime in (15% Er, 1% Nd):YAG is obtained from data such as that shown in Fig. 1 in which the log of the observed fluorescence intensity at 1.06 μm is plotted versus time. In such a plot an exponential decay process would appear as a straight line. However, the data are clearly not linear. These data were obtained by exciting the fluorescence with a frequency-doubled, *Q*-switched, Nd:YAG laser and monitoring its decay with a detector with response time < 1 μs. The fluorescence wavelength monitored was selected with a 0.25-m monochromator. The fluorescence signal was captured with a digital processing oscilloscope and 100 signals were averaged and processed with a computer to obtain results such as those shown in Fig. 1. The nonexponential decay indicated is real and not an artifact of the data acquisition and processing equipment. The entry for the lifetime in Table I was obtained from the 1/*e* decay time measured in the early, nearly exponential decay of the fluorescent intensity. As a check on this result we also measured the fluorescence decay at 1.34 μm since this transition also originates on the $^4F_{3/2}$ state of Nd^{3+}. The same nonexponential decay behavior was observed with the same initial 1/*e* decay time. The nonexponential decay behavior of Nd^{3+} in (Er, Nd):YAG is being studied further in continuing work.

In Nd:YAG, the lifetime of the $^4F_{3/2}$ state is nearly 240 μs and the decay process is governed by a single exponential mechanism. Clearly the presence of the Er^{3+} ions signifi-

TABLE I. Lifetimes of the states of Er and Nd in (Er, Nd:YAG) and Er in Er:YAG and Nd in Nd:YAG.

State	Material	Lifetime (ms)
$^4I_{11/2}$ of Er^{3+}	15% Er, 1% Nd:YAG	0.053 ± 0.004
$^4I_{11/2}$ of Er^{3+}	16.7% Er:YAG	0.107 ± 0.008
$^4I_{13/2}$ of Er^{3+}	15% Er, 1% Nd:YAG	0.081 ± 0.007
$^4I_{13/2}$ of Er^{3+}	16.7% Er:YAG	5.00 ± 0.1[a]
$^4F_{3/2}$ of Nd^{3+}	15% Er, 1% Nd:YAG	0.008 ± 0.0005[a]
$^4F_{3/2}$ of Nd^{3+}	1% Nd:YAG	0.237 ± 0.005

[a]These entries are the initial 1/*e* decay time of a process which does not appear to have a single exponential decay rate.

[a] Also at Allied Technologies, Westlake Village, CA 91362.

 0003-6951/87/421218-03$01.00

cantly alters the decay processes of the Nd^{3+} ions. Similarly the Nd^{3+} ions affect the Er^{3+} ions. The desired reduction of the Er^{3+} $^4I_{13/2}$ state lifetime has been achieved, although it is still longer than that of the $^4I_{11/2}$. One result of this is that the contribution of cross relaxation to the Er^{3+} $^4I_{11/2}$-$^4I_{13/2}$ inversion is considerably reduced with respect to that in Er:YAG. This can be understood since the cross relaxation rate is proportional to the square of the $^4I_{13/2}$ state population and this population does not grow as large as it would in Er:YAG. As seen in the lasing waveforms in Fig. 2, the phenomenon of quasicontinuous lasing is not observed for the 2.94-μm emission from (Er, Nd):YAG.

The lasing tests were performed with xenon flashlamp pumping in a silver-coated double-elliptical pump cavity. The pump pulse duration was 175 μs (full width at half-maximum) and the lamp arc length was 100 mm. Crystals of (15% Er, 1% Nd):YAG were grown by the Czochralski technique. Rods of 6.25 mm in diameter and 80 mm long were prepared. The tests reported in this letter were conducted with flat, parallel, and uncoated rod ends and 72 mm exposed to the pump light. The mirrors used were obtained from two different sources but had not been designed specifically for multiwavelength operation.[6] These were flat mirrors and they were spaced by 41 cm. In all cases the total reflector had measured reflectance of 99.7% at 2.94 μm and $>98.5\%$ in the 1-μm region.

When mirrors designed for reflection $>80\%$ at 2.94 μm were used, simultaneous lasing at 2.94 μm and in a band between 1.01 and 1.15 μm with a peak at 1.064 μm was detected. The lasing waveforms shown in Fig. 2 were obtained with a mirror designed for 90% reflection at 2.94 μm. The transmission of this mirror was 47% at 1.06 μm. Both waveforms were obtained with 550 J of pump energy into the lamps. This energy has been corrected to account for the difference in the arc and exposed rod lengths. This input corresponds to $5.1\times$ threshold for the 1.06-μm lasing and $4.5\times$ threshold for the 2.94-μm lasing. The only experimental difference between the two oscillographs is the setting of the 0.25-m monochromator used to distinguish between the lasing wavelengths. The waveforms were obtained with detectors having submicrosecond response times.

The laser and waveform detection system described in the preceding paragraph was used to detect lasing at 2.94 and 1.06 μm. In addition, clear evidence for laser emission from the (15% Er, 1% Nd):YAG (waveforms made up of relaxation spikes) was seen in a continuous band from 1.01 to 1.15 μm. The broadband was detected with mirrors designed for reflection at 2.94 μm as well as with mirrors designed for use at 1.06 μm. A Nd:YAG rod was inserted in the pump cavity and lased with the 65% R at 1.06 μm output mirror. This rod produced only the common 1.064-μm laser emission and no detectable broadband as seen with a doubly

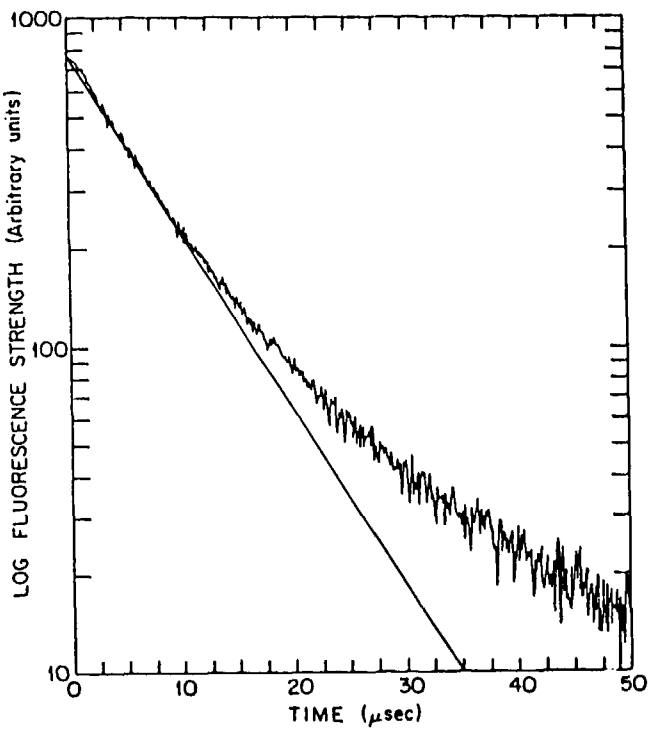

FIG. 1. Log of fluorescence signal decay vs time for the 1.06-μm emission from Nd^{3+} ions in (15% Er, 1% Nd):YAG.

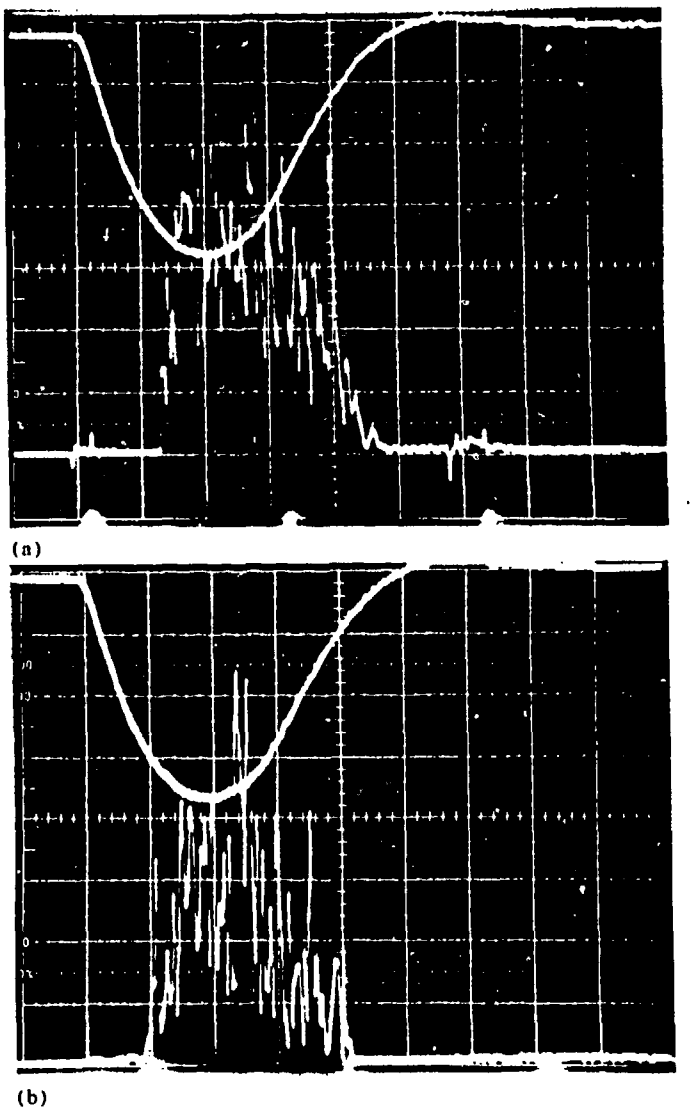

FIG. 2. Laser waveforms for the (a) 2.94 and (b) 1.06 μm signals from (15% Er, 1% Nd):YAG. These were obtained with 550 J to the flashlamps and are at $4.5\times$ and $5.1\times$ threshold, respectively. The horizontal scale for both waveforms is 50 μs/div.

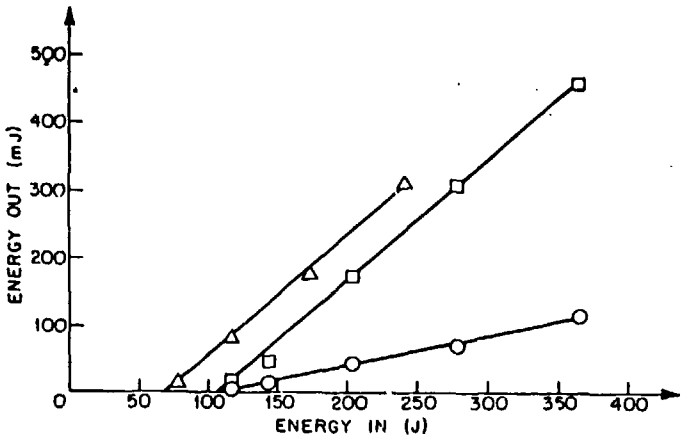

FIG. 3. Long pulse energy out vs energy in for (15% Er, 1% Nd):YAG. The input energy plotted is the total input to the flashlamps multiplied by 0.72 to account for the difference in arc and exposed rod length. (△) Data for 1 μm band lasing with the 65% R 1.06-μm mirror. (□) The 1-μm band output energy observed with a mirror designed for 90% R at 2.94 μm and which has 47% T at 1.06 μm. (○) Data for the 2.94-μm output using this mirror.

doped rod. This enabled calibration of the monochromator and demonstration that the instrumental bandwidth was $\pm$ 3 nm. If individual Nd^{3+} lines[7] were lasing to make up the band, the equipment would have resolved them into separate lines. The broadband of lasing contained a strong peak at 1.06 μm. Data are not yet available to resolve the energy distribution between the 1.06-μm line and the broadband and to determine the dependence of each on the mirror design. The broadband emission is another new feature of Nd^{3+} lasing observed in doubly doped (Er, Nd):YAG.

The long pulse output versus input energy of the (Er, Nd):YAG laser is plotted in Fig. 3. The abscissa is the total energy input to the flashlamps multiplied by 0.72 to account for the difference between the arc and exposed rod lengths. Data are shown for the case of the 90% R mirror described above and a standard 1.06-μm 65% R mirror. A calibrated filter which rejected light at 1 μm was used to enable measurement of the energy at 2.94 μm when both wavelengths were lasing. The 1-μm light energy shown in Fig. 3 is the difference between the measured 2.94-μm energy and the total energy measured with a calibrated joulemeter.

Simultaneous lasing by Er^{3+} and Nd^{3+} ions in doubly doped (Er, Nd):YAG was observed for the first time. Measurements of the state lifetimes of the ions in the doubly doped material indicate strong ion-ion interactions. These interactions result in unusual lasing properties such as the broadband of laser light detected in the 1.01–1.15 μm region. Work is in progress to more fully understand the interactions and to improve the lasing properties. This includes work with improved material, laser mirrors, and rod coatings, and attempts to tune the broadband emission. Other host and dopant combinations are being considered as possible members of this new class of multiple wavelength lasers.

This work was supported by the Air Force Office of Scientific Research under contract No. AFOSR-84-0378. Cooper Laser Sonics provided a gift to support this work. C. Enderby of Cooper Laser Sonics provided impetus to this work by suggesting that dual wavelength operation might occur and would be desirable for medical applications.

[1]E. V. Zharikov, V. I. Zhekov, L. A. Kulevskii, T. M. Murina, V. V. Osiko, A. M. Prokhorov, A. D. Savel'ev, V. V. Smirnov, B. P. Staridov, and M. I. Timoshechkin, Sov. J. Quantum Electron. 4, 1039 (1975).
[2]V. I. Zhekov, V. A. Lobachev, T. M. Murina, and A. M. Prokhorov, Sov. J. Quantum Electron. 13, 1235 (1983).
[3]M. Bass, W. Q. Shi, R. Kurtz, M. Kokta, and H. Diegl, in *Tunable Solid-State Lasers II*, edited by A. B. Budgor, L. Esterowitz, and L. G. DeShazer, Springer Series in Optical Sciences (Springer, Berlin, 1986), Vol. 52, pp. 300–305.
[4]A. A. Kaminskii, T. I. Butaeva, A. O. Ivanov, I. V. Mochalov, A. G. Petrosyan, G. I. Rogov, and V. A. Fedorov, Sov. Tech. Phys. Lett. 2, 308 (1976).
[5]A. A. Kaminskii, *Laser Crystals* (Springer, Berlin, 1981).
[6]Mirrors coated on sapphire substrates for specified 2.94 μm reflectivity were obtained from Rocky Mountain Instrument, 1501 S. Sunset Street, Longmount, CO 80501 and on ZnSe substrates from Laser Power Optics, 12777 High Bluff Drive, San Diego, CA 92130.
[7]J. Marling, IEEE J. Quantum Electron. QE-14, 56 (1978).

Simultaneous, multiple wavelength lasing of (Ho, Nd):$Y_3Al_5O_{12}$

J. Machan, R. Kurtz,[a] M. Bass, and M. Birnbaum
Center for Laser Studies, University of Southern California, Los Angeles, California 90089-1112
M. Kokta
Union Carbide Corporation, Washougal, Washington 98671

(Received 15 June 1987; accepted for publication 25 August 1987)

Simultaneous lasing of both Ho^{3+} and Nd^{3+} in the same crystal of yttrium aluminum garnet (YAG) is reported. The crystal was doped with 10% Ho^{3+} and 1% Nd^{3+} ions. Lasing occurred at 2.940 and 3.011 μm due to Ho^{3+} ion transitions and at 1.064 μm due to a Nd^{3+} transition. Appropriate mirrors produced simultaneous lasing at 1.064 and 1.339 μm due to Nd^{3+} ion transitions. The fluorescent lifetimes of both the Nd^{3+} $^4F_{3/2}$ and Ho^{3+} $^5I_7$ states were significantly lower in the doubly doped material than in Nd:YAG and Ho:YAG. This indicates very strong ion-ion interactions in the (Ho, Nd):YAG crystal.

Holmium has been reported to lase in yttrium aluminum garnet (YAG) in the 3-μm region.[1,2] This lasing is due to a transition from the Ho^{3+} $^5I_6$ to the $^5I_7$ level. However, the $^5I_7$ state has a much longer fluorescence lifetime than the $^5I_6$, and the lasing transition is self-terminated. Soviet researchers have observed this behavior in high-concentration holmium garnets and in yttrium orthoaluminate.[3] The (3.011 ± 0.003) μm lasing observed in our laboratory from 15% Ho:YAG clearly shows self-termination. This effect limits the duration of the laser pulse and the efficiency of the lasing process. Kaminskii *et al.* suggested that Nd^{3+} could be used to cross relax the Ho^{3+} $^5I_7$ level and thereby reduce or eliminate the problem of self-termination.[1] We have pursued this idea, and report, for the first time to our knowledge, on the multiwavelength lasing properties of a YAG crystal doped with 10% Ho^{3+} and 1% Nd^{3+} ions. Simultaneous laser action was observed at 2.940 and 3.011 μm by the Ho^{3+} ions, and at 1.064 μm by the Nd^{3+} ions. While the 3.011-μm wavelength has been reported in $Ho:YAlO_3$, we believe this is the first report of the 3.011-μm laser emission in YAG. By changing to mirrors which had nearly equal reflectance at 1.34 and 1.06 μm, simultaneous lasing was observed on both of these transitions, contrary to typical Nd:YAG laser properties.

The rationale behind the suggestion made by Kaminskii is seen by an examination of the energy levels of the Ho^{3+} and Nd^{3+} ions in YAG, shown in Fig. 1.[4] The laser transitions relevant to this work are indicated by the arrows. The Nd^{3+} $^4I_{13/2}$ level lies approximately 750 cm^{-1} below the Ho^{3+} $^5I_7$ state. This may allow energy transfer from the holmium to the neodymium ions, reducing the bottleneck which normally occurs as a result of the long $^5I_7$ lifetime. Measurements of the various state lifetimes involved in the Ho^{3+} laser transitions were made in 15% Ho:YAG and in (10% Ho, 1% Nd):YAG. The lifetime of the Nd^{3+} $^4F_{3/2}$ was determined in 1% Nd:YAG and in (10% Ho, 1% Nd):YAG. These data are listed in Table I. The drastically lower lifetimes of the Ho^{3+} $^5I_7$ and Nd^{3+} $^4F_{3/2}$ levels in the doubly doped material indicate that very strong interactions occur between the holmium and necdymium ions in this crystal.

The entries in Table I were obtained by exciting fluorescence in the crystals with a frequency-doubled, *Q*-switched Nd:YAG laser operating at 532 nm. Wavelength selection was accomplished using a 0.275-m monochromator, and the fluorescence decay was detected with a cooled InSb detector whose response time was < 1 μs. The monochromator was calibrated with the 1.064-μm emission from a Nd:YAG laser, and the instrumental bandwidth was found to be ± 0.003 μm. A digital processing oscilloscope recorded the fluorescence signals, which were then transferred to an HP9825A computer for storage and processing.

The lifetimes were derived from data such as those shown in Fig. 2, where the log of the fluorescence signal is plotted versus time. Up to 400 decay signals were averaged to obtain an improved signal-to-noise ratio. As Fig. 2 shows,

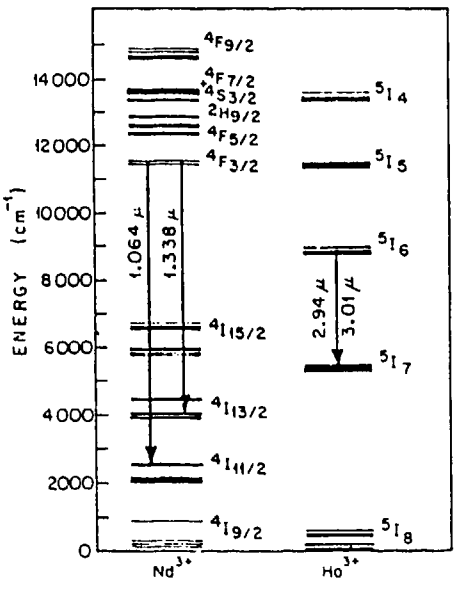

FIG. 1. Energy level diagram for Ho^{3+} and Nd^{3+} in YAG. Laser transitions are indicated by the arrows.

[a] Also at Allied Technologies, Westlake Village, CA 91362.

 0003-6951/87/431313-03$01.00

TABLE I. Lifetimes of the states of Ho^{3+} and Nd^{3+} in (Ho, Nd):YAG and Ho^{3+} in Ho:YAG and Nd^{3+} in Nd:YAG.

State	Material	Lifetime (μs)
$^5I_6$ of Ho^{3+}	15% Ho:YAG	47 ± 3
$^5I_6$ of Ho^{3+}	(10% Ho, 1% Nd):YAG	41 ± 3
$^5I_7$ of Ho^{3+}	15% Ho:YAG	5500 ± 500[a]
$^5I_7$ of Ho^{3+}	(10% Ho, 1% Nd):YAG	170 ± 10
$^4F_{3/2}$ of Nd^{3+}	1% Nd:YAG	237 ± 10
$^4F_{3/2}$ of Nd^{3+}	(10% Ho, 1% Nd):YAG	8.5 ± 0.8[a]

[a] These entries are the initial $1/e$ decay time of a process which does not appear to have a single exponential decay rate.

the Nd^{3+} $^4F_{3/2}$ decay in (Ho, Nd):YAG is nonexponential, exhibiting a continuous curvature. This continuous change in the decay rate of the fluorescence was followed out to beyond 200 μs by using appropriate delays on the oscilloscope. The value given for the decay time in Table I is the initial $1/e$ decay time. This behavior was observed from 1.064 and 1.339 μm emission, which both originate from the $^4F_{3/2}$ level. The decrease in the Nd^{3+} lifetime is evidence of significant energy transfer from Nd^{3+} to Ho^{3+} in this crystal.

The Ho^{3+} $^5I_6$ lifetime has been reduced by only 15% due to the presence of the Nd^{3+}, while the $^5I_7$ lifetime was reduced by a factor of 30 or more, as shown in Table I. The decay of Ho^{3+} $^5I_7$ in 15% Ho:YAG is nonexponential. It was not possible to precisely measure the Ho^{3+} $^5I_5$ lifetime due to detector sensitivity and response time. However, the data that were obtained showed that the lifetime of this level was < 5 μs. The decay processes are being studied further.

All lasing tests were conducted in a silver-coated double-elliptical pump cavity with xenon flashlamps. The arc length was 100 mm with a pump pulse duration of 175 μs full width at half-maximum. Due to the short upper level lifetimes of both Nd^{3+} and Ho^{3+} in (10% Ho, 1% Nd):YAG the long pump pulse may have resulted in inefficient pumping. The laser material was grown using the Czochralski technique. A rod 6.35 mm in diameter and 70 mm in length was used, although the pumped rod length was 64 mm. The input energies in Fig. 3 represent energy input to the lamps, corrected for the mismatch between arc and pumped rod lengths. The rod was prepared with flat, parallel, uncoated faces. Several mirror sets were used for the lasing tests, but none was specifically designed for multiwavelength operation. All mirrors used were flat.

When a mirror designed for 90% reflection at 2.94 μm was used in conjunction with an enhanced silver total reflector designed for 100% reflection at 2.94 μm, simultaneous lasing was observed at 2.940, 3.011, and 1.064 μm (all are ± 0.003 μm), with the output energies indicated in Fig. 3. A temporal shift of the lasing from 2.940 to 3.011 μm was observed. This is similar to that reported by Soviet researchers for Ho^{3+} and Er^{3+} in other hosts.[3,5] The 2.940-μm lasing always precedes the 3.011-μm transition in time. Due to the longer lifetime of the lower state, the lower Stark levels fill during the initial lasing process and the gain decreases. Lasing then switches to the longer wavelength transition. Ho^{3+} lasing at 3.011 μm has not previously been reported in YAG.

For comparison, in 15% Ho:YAG, only the 3.011-μm emission was obtained, and all lasing ceased prior to the peak of the pump pulse. This is in contrast to the (Ho, Nd):YAG, where 3.011 μm emission switched on near the end of the 2.940-μm lasing, and continued past the peak of the pump. A combined total output energy of 41 mJ was obtained from the (10% Ho, 1% Nd):YAG material at 2.940 and 3.011 μm with 540 J input to the lamps (340 J corrected for length mismatch). This was significantly more than could be obtained from a longer and higher quality laser rod of 15% Ho:YAG operated under identical conditions.

More unusual lasing properties were found when the 2.94-μm output coupler was replaced with a mirror which had a reflectivity of 90% at 1.34 μm and 88% at 1.06 μm.

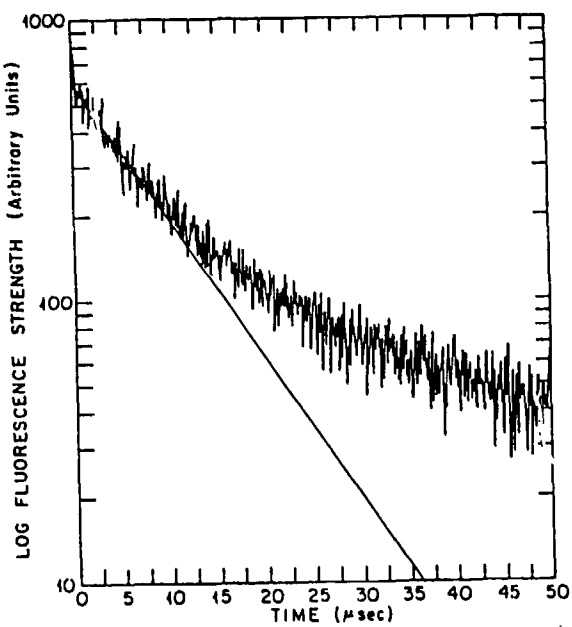

FIG. 2. Log of fluorescence signal decay vs time for the 1.06-μm emission from the Nd^{3+} $^4F_{3/2}$ level in (10% Ho, 1% Nd):YAG.

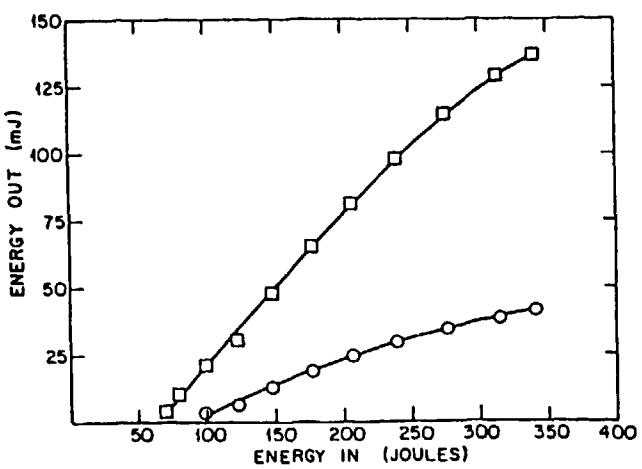

FIG. 3. Long pulse energy out vs energy in for (10% Ho, 1% Nd):YAG. The input energy plotted is the input to the flashlamps corrected for the mismatch in arc and exposed rod length. The output coupler used was designed for 90% reflectance at 2.94 μm and had a transmission of 3% at 1.06 μm. Reflectance at 1.34 μm was less than 10%. Circles are combined energy at 2.940 and 3.011 μm. Squares are output energy at 1.064 μm.

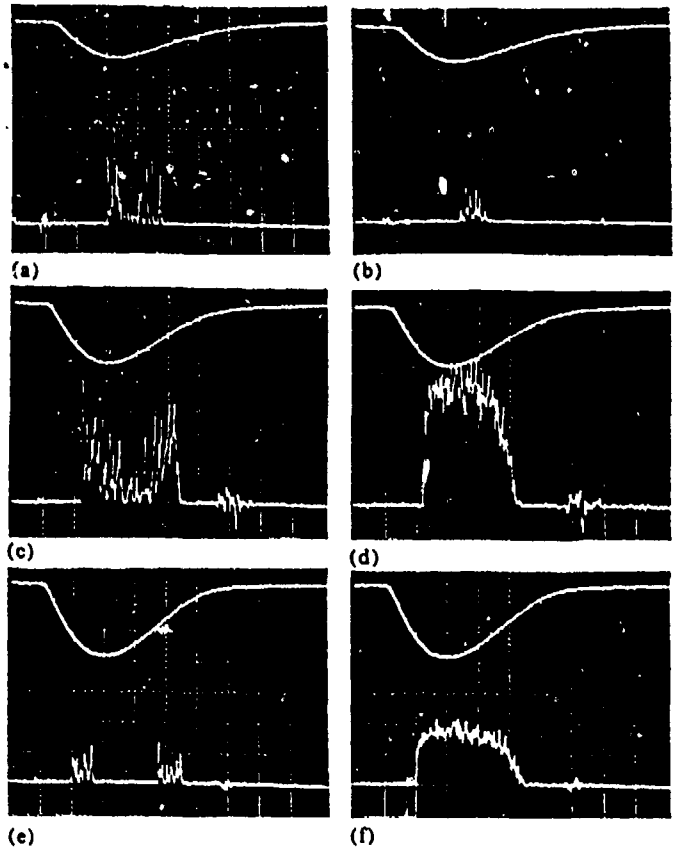

FIG. 4. Laser waveforms for the Nd^{3+} 1.339 and 1.064 μm signals from (10% Ho, 1% Nd):YAG. The upper trace monitors the current pulse to the flashlamps. The horizontal scale is 50 μs/div in all oscillographs. Waveforms at 1.339 (a) and 1.064 μm (b) with 69 J (corrected) input. Vertical scale is 10 mV/div. Waveforms at 1.339 (c) and 1.064 μm (d) with 148 J (corrected) input. Vertical scale is 20 mV/div. Waveforms at 1.339 (e) and 1.064 μm (f) with 207 J (corrected) input. Vertical scale is 50 mV/div.

This mirror combination produced simultaneous lasing at 1.064 and 1.339 μm. The unique temporal behavior of this lasing is illustrated in Fig. 4. The 1.339-μm transition has a lower threshold than the 1.064-μm [see Figs. 4(a) and 4(b)]. As the input energy is increased the 1.064-μm output rapidly becomes more intense, and the 1.339-μm lasing only occurs at the leading and trailing edges of the 1.064-μm lasing [see Figs. 4(c)–4(f)]. This may result from the residual absorption of holmium at 1.064 μm. Although small, it is apparently sufficient to alter the threshold condition for the two transitions, allowing 1.339 μm lasing to occur at low pump levels. It is possible that at higher inputs the inversion is large enough to enable 1.064 μm lasing and this transition then competes successfully with the 1.339-μm transition for the inversion.

When the total reflector was changed to one which had a maximum reflectivity at 1.34 μm and $R < 40\%$ at 1.06 μm, only 1.339 μm lasing was observed with no temporal breakup of the pulse. The maximum energy out of the rod at 1.339 μm under these conditions was 260 mJ.

In this initial work, no attempt was made to optimize any of the parameters involved to maximize output at a particular wavelength. The concentrations of the dopants can be varied, and different host crystals are being considered to improve the performance of this dopant combination. Improved material and an optimization of mirror reflectivities at the various wavelengths involved are expected to increase lasing performance. Work is in progress to understand the ion-ion interactions in this material. Such multiple wavelength lasers have potential for medical, military, and scientific applications.

Simultaneous lasing by Ho^{3+} and Nd^{3+} ions has been observed in doubly doped (Ho, Nd):YAG for the first time. Strong ion-ion interactions are indicated by the drastic changes in the Nd^{3+} $^4F_{3/2}$ and Ho^{3+} $^5I_7$ lifetimes. These interactions produce more efficient 3 μm lasing from Ho^{3+}, and some unusual lasing properties from Nd^{3+}, as 1.064 and 1.339 μm lasing occur simultaneously. With appropriate mirrors, it is believed that all four wavelengths would lase at the same time.

This work was supported by the Air Force Office of Scientific Research under contract No. AFOSR-84-0373. Cooper Laser Sonics provided a gift to support this work. C. Enderby of Cooper Laser Sonics provided impetus to this work by suggesting that dual wavelength operation might occur in (Er, Nd):YAG and would be desirable for medical applications. Valuable discussions with W. Q. Shi are also acknowledged.

[1] A. A. Kaminskii, T. I. Butaeva, A. O. Ivanov, I. V. Mochalov, A. G. Petrosyan, G. I. Rogov, and V. A. Fedorov, Sov. Tech. Phys. Lett. 2, 308 (1976).
[2] M. Kh. Ashurov, Yu. K. Voron'ko, E. V. Zharikov, A. A. Kaminskii, V. V. Osiko, A. A. Sobol', M. I. Timoshechkin, V. A. Fedorov, and A. A. Shabaltai, Inorg. Mater. 15, 979 (1979).
[3] A. A. Kaminskii, V. A. Fedorov, and I. V. Mochalov, Sov. Phys. Dokl. 25, 744 (1980).
[4] A. A. Kaminskii, *Laser Crystals* (Springer, Berlin, 1981).
[5] A. A. Kaminskii, V. A. Fedorov, A. O. Ivanov, I. V. Mochalov, and L. I. Krutova, Sov. Phy. Dokl. 27, 725 (1982).

Investigation of the interactions between dissimilar ions in (Er, Nd):$Y_3Al_5O_{12}$

W. Q. Shi, M. Bass,* and M. Birnbaum

Center for Laser Studies, University of Southern California, Los Angeles, California 90089-1112

Received March 8, 1988; accepted September 22, 1988

Unusual fluorescence decay properties of both Er^{3+} and Nd^{3+} ions in (Er, Nd):YAG are reported. Studies reveal that the cross-relaxation-type ion–ion interactions involving Er^{3+} and Nd^{3+} ions are responsible. A rate-equation analysis is used to evaluate the interaction strengths of all the proposed processes. The rate-equation calculation does not fully explain the nonexponential nature of the measured fluorescence decay function of the $^4F_{3/2}$ Nd^{3+} ions. As a result, the theory for donor–acceptor energy transfer processes, based on the inverse-power transfer rate model, is adopted to study the mechanism of the interactions between Er^{3+} and Nd^{3+} ions that result in the drastically altered fluorescence decay of Nd^{3+} ions. It is found that the mechanisms governing the energy transfer processes have functional forms different from those for the commonly encountered electric multipolar interactions. The interaction strengths are evaluated by least-squares fitting of the theory to the experimental data. Effects of the ion–ion interactions on lasing properties of the (Er, Nd):YAG are also discussed.

INTRODUCTION

Lasing at 2.94 μm from highly doped Er:YAG provides an efficient and useful coherent light source. Because the lower level of this laser transition has a longer decay lifetime than the upper level, the laser action at 2.94 μm is self-terminated. As a result of this bottleneck, the flash-lamp-pumped Er:YAG laser has been unable to lase in the cw mode, although quasi-cw lasing has been observed from this laser crystal.[1,2] In an earlier paper,[3] we reported our work on yttrium aluminum garnet doubly doped with 15 at. % Er^{3+} and 1 at. % Nd^{3+} ions. In this material, Nd^{3+} ions were added to the Er:YAG crystal in order to relax the Er^{3+} $^4I_{13/2}$ state through energy transfer between Er^{3+} and Nd^{3+} ions, as Kaminskii *et al.* suggested in Ref. 4. This process can be effective because the Er^{3+} $^4I_{13/2}$ and Nd^{3+} $^4I_{15/2}$ states are almost isoenergetic in YAG.[5] In the same paper we also described the large reductions in the Er^{3+} $^4I_{13/2}$ and Nd^{3+} $^4F_{3/2}$ lifetimes and the simultaneous laser action of both Er^{3+} and Nd^{3+} ions. Here we describe in more detail the unusual fluorescence decay properties of (Er, Nd):YAG. A rate-equation model has been proposed, including cross-relaxation processes between like and unlike ions, and a theory for the donor–acceptor energy transfer processes has been used to analyze the interaction mechanisms. Effects of these processes on fluorescence decay and lasing properties of the material are discussed.

OBSERVATION OF FLUORESCENCE DECAY PROPERTIES OF (Er, Nd):YAG

The fluorescence decay of the lasing levels is one of the most important characteristics of a laser material. To explore the fluorescence decay properties and to reveal the ion–ion interaction mechanisms in (Er, Nd):YAG, experiments were carefully conducted to observe the fluorescence decay from various energy states of both Er^{3+} and Nd^{3+} ions in this material. The sample used in the experiments was a YAG crystal doped with 15 at. % Er and 1 at. % Nd ions. The states from which fluorescence emission was monitored are the Er^{3+} $^4I_{11/2}$, Er^{3+} $^4I_{13/2}$, and Nd^{3+} $^4F_{3/2}$ states. The fluorescence decay properties of the Er^{3+} $^4I_{11/2}$ and $^4I_{13/2}$ states, between which the 2.94-μm lasing emission occurred, were revealed through the ~1.007-μm ($^4I_{11/2} \rightarrow {}^4I_{15/2}$) and ~1.63-$\mu$m ($^4I_{13/2} \rightarrow {}^4I_{15/2}$) transition lines, respectively. Those of the Nd^{3+} $^4F_{3/2}$ state were studied through the popular 1.06-μm ($^4F_{3/2} \rightarrow {}^4I_{11/2}$) line. In our experiments the sample was excited with a Q-switched, frequency-doubled Nd:YAG laser, and the fluorescence transition lines were isolated with a 0.27-m Jarrell-Ash single-grating monochromator. The fluorescence light from the monochromator was collected by a liquid nitrogen-cooled InSb IR detector. The output signals from the detector were stored and processed by a computer-controlled data acquisition system, which could average any preset number of signals for noise reduction. The experimental results obtained are shown in Figs. 1–3. The unusual fluorescence decay properties of the (Er, Nd):YAG crystal are compared with the decay curves of the same states in singly doped 16.6 at. % Er:YAG or 1 at. % Nd:YAG (Figs. 1–3). From Figs. 1–3, the following features were observed:

(1) For the Er^{3+} $^4I_{11/2}$ state (Fig. 1): Fluorescence decay from the singly doped Er:YAG starts out to be linear in a semilog plot that corresponds to an exponential decay and then gradually curves up, which is indicative of a decrease in decay rate. The initial $1/e$ decay time is 106 μsec, which corresponds to the measured decay lifetime of the Er^{3+} $^4I_{11/2}$ state in 1 at. % Er:YAG. This nonexponential decay has been demonstrated[6,7] to be a result of cross-relaxation processes in Er:YAG. It has also been shown[6,7] that simple exponential fluorescence decay of the Er^{3+} $^4I_{11/2}$ and $^4I_{13/2}$ states in Er:YAG could be obtained at low excitation levels when the cross-relaxation processes were not effective. Us-

0740-3224/89/010023-07$02.00

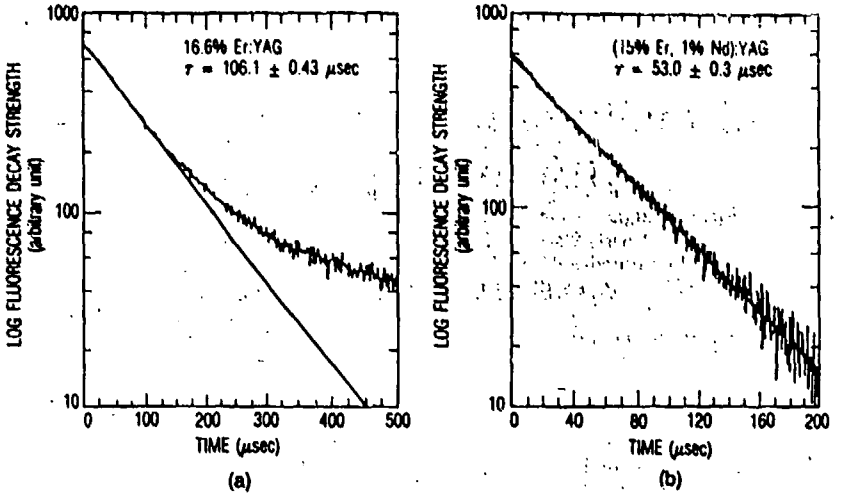

Fig. 1. Experimentally observed decay curves from Er^{3+} $^4I_{11/2}$ in (a) 16.6% Er:YAG, (b) (15% Er, 1% Nd):YAG.

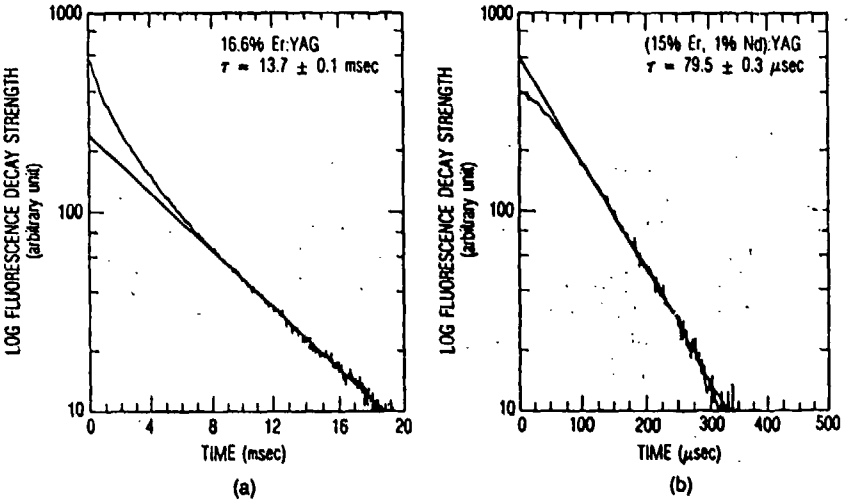

Fig. 2. Experimentally observed decay curves from Er^{3+} $^4I_{13/2}$ in (a) 16.6% Er:YAG, (b) (15% Er, 1% Nd):YAG.

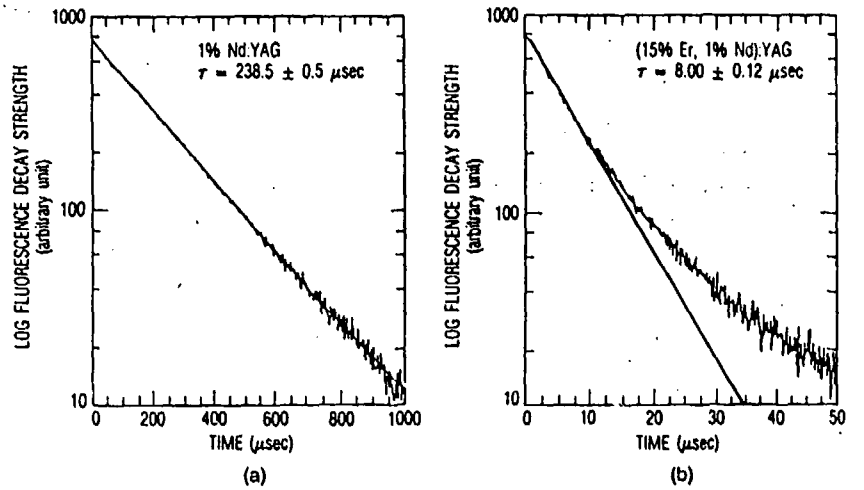

Fig. 3. Experimentally observed decay curves from Nd^{3+} $^4F_{3/2}$ in (a) 1% Nd:YAG, (b) (15% Er, 1% Nd):YAG.

Table 1. Observed Fluorescence Decay Properties of (Er, Nd):YAG

State	Observations
Er^{3+} $^4I_{11/2}$	Decay is governed by a simple exponential and is two times faster than in Er:YAG.
Er^{3+} $^4I_{13/2}$	Decay shows slow filling at early times (first 50 μsec), then becomes an exponential and is approximately 170 times faster than in Er:YAG.
Nd^{3+} $^4F_{3/2}$	Decay is an exponential at early stage (first 10 μsec) and is 30 times faster than in Nd:YAG; later it becomes slower and nonexponential.

ing this method, we were able to measure the fluorescence decay lifetime of the Er^{3+} $^4I_{11/2}$ state in Er:YAG as a function of Er concentration. It was found[6,7] that this lifetime was independent of Er concentration, indicating that the Er^{3+} $^4I_{11/2}$ state in Er:YAG was not subject to concentration quenching.

In comparison, the (Er, Nd):YAG shows a decay governed by a simple exponential over nearly four e-folding periods, independent of pump levels. Another important feature of the decay from the Er^{3+} $^4I_{11/2}$ state in (Er, Nd):YAG is that the $1/e$ decay time (53 μsec) is only one half of that of Er:YAG.

(2) For the Er^{3+} $^4I_{13/2}$ state (Fig. 2): The decay curves of the Er^{3+} $^4I_{13/2}$ state in Er:YAG [Fig. 2(a)] and (Er, Nd):YAG [Fig. 2(b)] differ strikingly in that the decay in (Er, Nd):YAG is approximately 170 times faster than that in Er:YAG. This observation confirms the expected reduction of the Er^{3+} $^4I_{13/2}$ level lifetime. The nonexponential decay of the Er^{3+} $^4I_{13/2}$ state in Er:YAG is due to the cross-relaxation processes as discussed in feature (1) above. Simple exponential decay was obtained by using low excitation, which allowed us to measure the decay lifetime of the Er^{3+} $^4I_{13/2}$ state in Er:YAG. This lifetime was found to be 13.7 msec for 16.6 at. % Er:YAG. In addition, the Er^{3+} $^4I_{13/2}$ state in (Er, Nd):YAG, whose decay pattern was independent of excitation levels, shows a slow decrease in fluorescence strength at the initial stage of the decay.

(3) For the Nd^{3+} $^4F_{3/2}$ state (Fig. 3): In Nd:YAG the lifetime of the $^4F_{3/2}$ state is approximately 240 μsec, and the decay process is governed by a simple exponential. However, in (Er, Nd):YAG not only is nonexponential decay of the Nd^{3+} $^4F_{3/2}$ state observed but an initial $1/e$ decay time of approximately 8 μsec is recorded. To check this observation and ensure that it is not an artifact of the data acquisition and processing equipment, we also monitored the fluorescence decay at 1.34 μm, which corresponds to the Nd^{3+} transition from the $^4F_{3/2}$ to $^4I_{13/2}$ states. The same nonexponential decay behavior was observed with the same initial $1/e$ decay time.

As we pointed out in our earlier paper,[3] the drastically altered fluorescence decay rates suggest significant unlike ion–ion interactions in the (Er, Nd):YAG crystal. In the section that follows we discuss theoretical models of the ion–ion interactions as applied to the system under study; these models provide a basic understanding of the mechanisms that result in the observations described above. A summary of the observed fluorescence decay properties from the three Er^{3+} and Nd^{3+} states is listed in Table 1.

THEORETICAL INVESTIGATION OF THE MECHANISMS OF THE ION-ION INTERACTIONS IN (Er, Nd):YAG

To understand the physical processes responsible for the observations described above, we introduced three cross-relaxation processes that involve both Er^{3+} and Nd^{3+} ions. These processes are depicted in Fig. 4, along with the known decay and energy exchange processes. Strong relaxation processes are expected because both energy-state pairs involved in each of the three processes have the same energy difference. A rate-equation analysis, which includes the cross-relaxation processes shown in Fig. 4, was used to calculate the time-varying population distribution of the coupled Er^{3+} and Nd^{3+} states from which fluorescence decays were observed. The coupled rate equations were solved numerically by utilizing the fifth- and sixth-order Runge Kutta–Verner method, and the results were compared with the observed decay data.

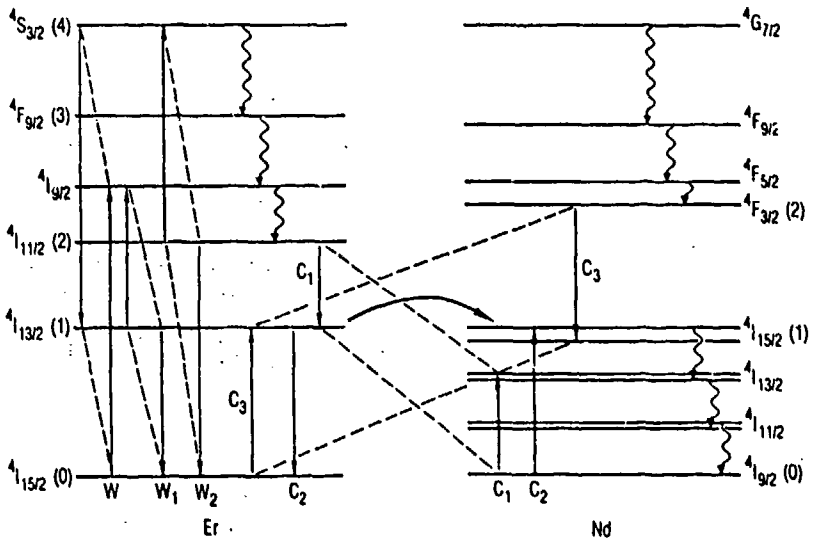

Fig. 4. Ion–ion interaction and relaxation processes in (Er, Nd):YAG.

With reference to Fig. 4, W, W_1, and W_2 describe cross-relaxation processes of the Er^{3+} ions in high dopant density Er^{3+}-doped materials. They are responsible for the nonexponential decay of the Er^{3+} $^4I_{11/2}$ and $^4I_{13/2}$ states [Figs. 1(a) and 2(a)] and the quasi-cw laser operation in the 3-μm region of high-concentration Er^{3+}:YAG lasers.[1,6] C_1, C_2, and C_3 in Fig. 4 represent the cross-relaxation processes proposed to account for the drastically altered fluorescence decay functions observed in (Er, Nd):YAG. With reference to Table 1 and Fig. 4, we introduce the following:

(1) The process described by C_1 to account for the faster decay of the Er^{3+} $^4I_{11/2}$ state.

(2) The process described by C_2 to account for the faster decay of the Er^{3+} $^4I_{13/2}$ state and the simple exponential decay of the Er^{3+} $^4I_{11/2}$ state.

(3) The process described by C_3 to account for the faster decay of the Nd^{3+} $^4F_{3/2}$ state and the filling of the $^4F_{3/2}$ state Nd^{3+} ions during the early stage of the Er^{3+} $^4I_{13/2}$ decay.

C_1, C_2,and C_3 are the cross-relaxation coefficients and were assumed to be constant in time in our model. The Er^{3+} energy states under consideration are $^4S_{3/2}$ + $^2H_{11/2}(4)$, $^4F_{9/2}(3)$, $^4I_{11/2}(2)$, $^4I_{13/2}(1)$, and $^4I_{15/2}(0)$, and those of Nd^{3+} ions are $^4F_{3/2}(2)$, $^4I_{15/2}(1)$, and $^4I_{9/2}(0)$. The numbers in parentheses are those used to label the energy states of each kind of ion (see Fig. 4).

A set of rate equations is presented below, which includes the various cross-relaxation processes among like or unlike ions in addition to spontaneous emission, multiphonon transitions, and external excitation. The equations involving Er^{3+} states were normalized with respect to the Er^{3+} concentration (C^{Er}), and those dealing with Nd^{3+} states were normalized with respect to the Nd^{3+} concentration (C^{Nd}). This is why C^{Er} and C^{Nd} appear explicitly in the equations. Assume that the initial conditions are $n_0^{Er}(t=0)=1$; $n_i^{Er}(t=0)=0$, where $i=1,2,3,4$; and $n_0^{Nd}(t=0)=1$, $n_i^{Nd}(t=0)=0$, where $i=1,2$. Then the resulting set of eight coupled equations is

$$\frac{dn_0^{Er}}{dt} = -W_{04}n_0^{Er} + \frac{n_1^{Er}}{\tau_1^{Er}} - (n_0^{Er}W)n_4^{Er} + (C^{Er}W_1)(n_1^{Er})^2 + (C^{Er}W_2)(n_2^{Er})^2 - C_3n_2^{Nd}n_0^{Er}C^{Nd} + C_2n_1^{Er}n_0^{Nd}C^{Nd}, \quad (1)$$

$$\frac{dn_1^{Er}}{dt} = \frac{n_2^{Er}}{\tau_2^{Er}} - \frac{n_1^{Er}}{\tau_1^{Er}} + (n_0^{Er}W)n_4^{Er} - (2C^{Er}W_1)(n_1^{Er})^2 - C^{Nd}C_2n_1^{Er}n_0^{Nd} + C^{Nd}C_3n_2^{Nd}n_0^{Er} + C_1n_2^{Er}n_0^{Nd}C^{Nd}, \quad (2)$$

$$\frac{dn_2^{Er}}{dt} = \frac{n_3^{Er}}{\tau_3^{Er}} - \frac{n_2^{Er}}{\tau_2^{Er}} + (n_0^{Er}W)n_4^{Er} + (C^{Er}W_1)(n_1^{Er})^2 - (2C^{Er}W_2)(n_2^{Er})^2 - C^{Nd}C_1n_2^{Er}n_0^{Nd}, \quad (3)$$

$$\frac{dn_3^{Er}}{dt} = W_{43}^{mp}n_4^{Er} - \frac{n_3^{Er}}{\tau_3^{Er}}, \quad (4)$$

$$\frac{dn_4^{Er}}{dt} = W_{04}n_0^{Er} - \frac{n_4^{Er}}{\tau_4^{Er}} + (C^{Er}W_2)(n_2^{Er})^2, \quad (5)$$

$$\frac{dn_0^{Nd}}{dt} = \frac{n_1^{Nd}}{\tau_1^{Nd}} - W_{02}n_0^{Nd} + \frac{n_2^{Nd}}{\tau_2^{Nd}} - C^{Er}C_2n_1^{Er}n_0^{Nd}, \quad (6)$$

$$\frac{dn_1^{Nd}}{dt} = C^{Er}C_2n_1^{Er}n_0^{Nd} - \frac{n_1^{Nd}}{\tau_1^{Nd}} + C^{Er}C_3n_2^{Nd}n_0^{Er}, \quad (7)$$

$$\frac{dn_2^{Nd}}{dt} = W_{02}n_0^{Nd} - \frac{n_2^{Nd}}{\tau_2^{Nd}} - C^{Er}C_3n_2^{Nd}n_0^{Er}, \quad (8)$$

where

C^{Er} is the concentration of Er^{3+} ions;
C^{Nd} is the concentration of Nd^{3+} ions;
W_{04} and W_{02} are the external excitation rates;
n_i^{Er} is the normalized population of the ith Er^{3+} state;
n_i^{Nd} is the normalized population of the ith Nd^{3+} state;
τ_i^{Er} is the fluorescence decay lifetime of the ith Er^{3+} state;
τ_i^{Nd} is the fluorescence decay lifetime of the ith Nd^{3+} state;
C_i is the coefficient of the ith ion–ion interaction process, $i=1,2,3$;
W_{43}^{mp} is the multiphonon transition rate from 4 to 3 of Er^{3+} ions;
$n_0^{Er}W$ is the cross-relaxation rate of the Er $^4S_{3/2}$ level;
$W_1(W_2)$ is the cross-relaxation coefficient for the cross-relaxation process originating from the Er^{3+} $^4I_{13/2}(^4I_{11/2})$ state.

Several assumptions have been made in writing these equations. They are as follows:

(1) The Nd^{3+} energy levels above the $^4F_{3/2}$ relax so fast through phonon-assisted processes that the Nd^{3+} $^4F_{3/2}$ level is effectively directly pumped (a four-level system).

(2) Energy transfer from the Nd^{3+} $^4I_{15/2}$ level to the Er^{3+} $^4I_{13/2}$ level is negligible compared with the phonon-assisted relaxation of the Nd^{3+} $^4I_{15/2}$ level.

(3) $A_{4j}^{Er} \ll W_{43}^{mp}$, and $n_0^{Er}W$ is therefore neglected.

(4) $A_{3j}^{Er} \ll W_{32}^{mp}$ and therefore is neglected.

(5) $A_{2j} \ll W_{21}^{mp}$, and the cross-relaxation rate W_2 is therefore neglected. [Note that $\eta_{qe}(Er^{3+}\ ^4I_{11/2})$ is less than 1.5%.[8]]

Here A_{ij}^{Er} is the radiative transition rate from the Er^{3+} state i to state j, and W_{ij}^{mp} is the multiphonon transition rate from the Er^{3+} state i to state j.

Our primary objective was to show the validity of our model by comparing the results of the calculation with the experimental data. An iterative fitting procedure leads to the determination of the cross-relaxation coefficients C_1, C_2,and C_3, which are the only unknown parameters in the equations.

Numerical solutions of the rate equations were obtained by the fifth- and sixth-order Runge Kutta–Verner method.[9] The results are plotted in Figs. 5 and 6, in which they are compared with the observed decay data. The parameters used for obtaining the results are listed in Table 2, and the fitted values for the cross-relaxation coefficients C_1, C_2, and C_3 are summarized in Table 3.

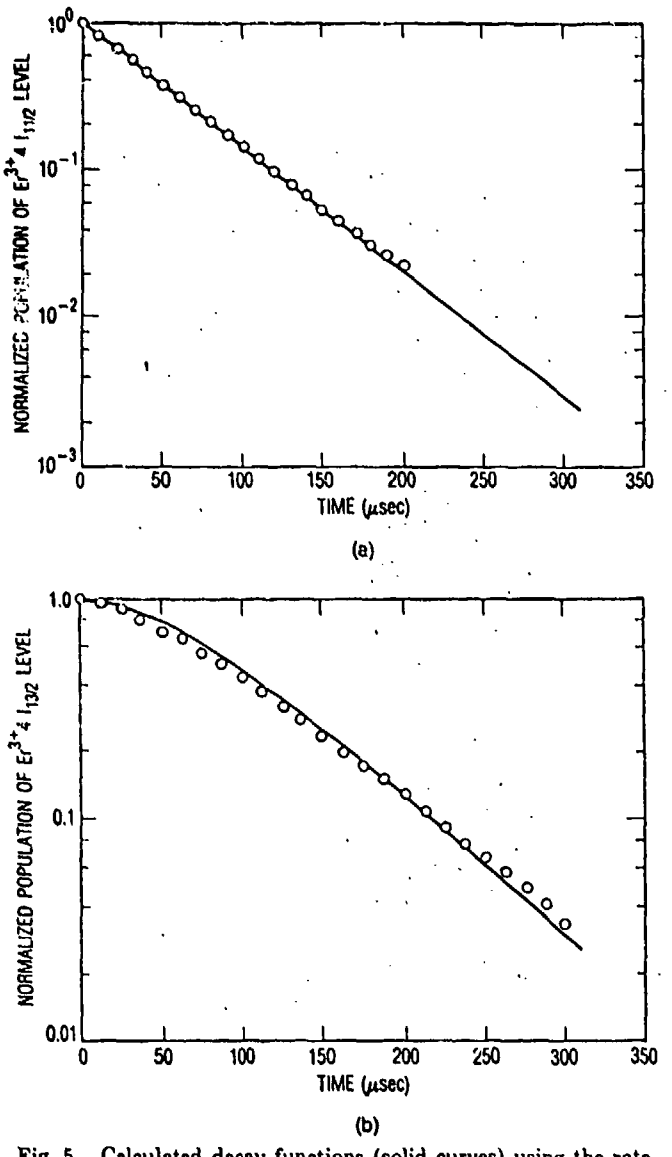

Fig. 5. Calculated decay functions (solid curves) using the rate-equation analysis of (a) the Er^{3+} $^4I_{11/2}$ state and (b) the Er^{3+} $^4I_{13/2}$ state as compared with experimental data (circles).

From Figs. 5(a) and 5(b), we see that the computed curves agree well with the observed Er^{3+} decay curves, indicating that the proposed cross-relaxation processes and coefficients are appropriate for the unlike ion–ion interactions in this crystal. However, in Fig. 6 a discrepancy was observed between the calculation (solid, straight line) and experimental data for the Nd^{3+} $^4F_{3/2}$ decay. This, however, by no means suggests that the process governed by C_3, shown in Fig. 4, does not function as it should. The importance of such a process is indicated by the fact that including the process governed by C_3 can explain the slow filling in the early stage of the Er^{3+} $^4I_{13/2}$ state decay, as Fig. 5(b) shows. The difference between calculation and experiment in Fig. 6 comes about because a constant interaction strength was assumed in the calculation. In reality this may not be true because not all Nd^{3+} sites provide the same strength of interaction with Er^{3+} ions in a sample that has 15 at. % Er^{3+} ions but only 1 at. % Nd^{3+} ions. In this case one Nd^{3+} ion can see a spatial distribution of Er^{3+} ions around it, and some Er^{3+} ions may interact with this Nd^{3+} ion with a strength that is different from the strength of interaction between this Nd^{3+} ion and another group of Er^{3+} ions. The overall effect of interactions of this nature is to give rise to the nonexponential decay of the Nd^{3+} $^4F_{3/2}$ state. In the YF_3:Yb, Ho system, for example, similar nonexponential decay was observed from the Yb^{3+} ions that was due to the energy transfer from Yb^{3+} ions to Ho^{2+} ions.[13]

Because of the difficulty of incorporating a nonconstant interaction strength between Nd^{3+} and Er^{3+} ions, we will use the analytical expression for the donor luminescence of a donor–acceptor system, as derived by Inokuti and Hirayama[14] on the basis of the Förster–Dexter theory of energy transfer,[15,16] in order to investigate the mechanisms governing the Nd^{3+} $^4F_{3/2}$ decay in (Er, Nd):YAG under study.

We begin our analysis with the assumption that the energy diffusion effect among excited Nd^{3+} ions is negligible. This is justified by the fact that our sample contains 1 at. % Nd^{3+} ions, and the excited Nd^{3+} ions in 1 at. % Nd:YAG have a high quantum efficiency. Therefore the mechanism under consideration is energy transfer between donor (excited Nd^{3+}) –acceptor (ground-state Er^{3+}) pairs.

The total rate of transfer from an excited donor to an acceptor at a distance R can be expressed as

$$W_T(R) = \frac{1}{\tau_0} + n(R), \tag{9}$$

where τ_0 is the intrinsic lifetime of the excited donors and $n(R)$ is the energy transfer rate of a donor–acceptor pair whose two ions are a distance R from each other. If the energy transfer is governed by a particular electric multipolar term, the transfer rate can be written as

$$n(R) = \frac{1}{\tau_0}\left(\frac{R_0}{R}\right)^s, \tag{10}$$

where s is a positive number and R_0 is, according to Förster,[15] a critical transfer distance such that the transfer rate $n(R)$ is equal to the intrinsic decay rate $1/\tau_0$ of the donor when R is equal to R_0. Using this model (sometime referred to as the inverse-power rate model), Inokuti and Hiragama[14] were

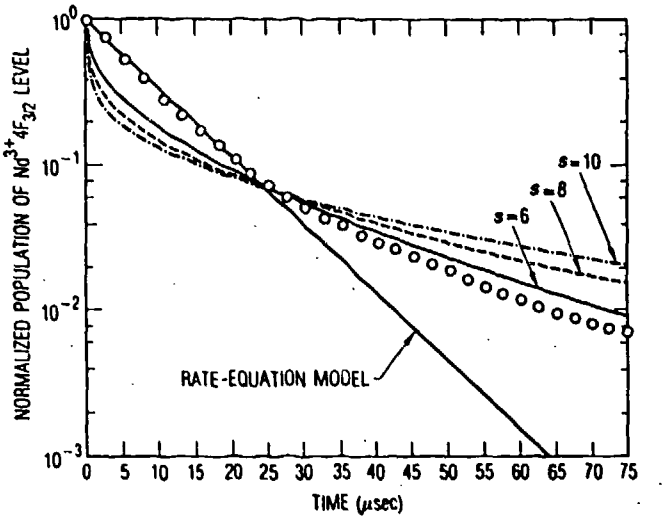

Fig. 6. Decay functions of the $^4F_{3/2}$ Nd^{3+} ions calculated by using the rate-equation model (solid, straight line) and energy transfer theory compared with the experimental data (circles).

Table 2. Parameters Used in Rate-Equation Calculation

Parameters	Values	Reference
C^{Er}	2.1×10^{21} cm^{-3} (15 at. %)	a
τ_1^{Er}	13.7 msec	a
τ_2^{Er}	106 μsec	a
τ_3^{Er}	1.2 μsec	6
τ_4^{Er}	1.0 μsec	6
W_{43}^{mp}	1.8×10^5 sec^{-1}	10
$n_0^{Er}W$	9.3×10^5 sec^{-1}	10
W_1	2.5×10^{-17} cm^3/sec	6
W_2	5.0×10^{-17} cm^3/sec	6
C^{Nd}	1.38×10^{20} cm^{-3}(1 at. %)	11
τ_1^{Nd}	~2 μsec	12
τ_2^{Nd}	237 μsec	a

[a] Our results.

Table 3. Cross-Relaxation Coefficients for Unlike Ion–Ion Interaction Processes in (Er, Nd):YAG

Coefficients	Values ($\times 10^{-16}$ cm^3/sec)
C_1	0.7
C_2	1.2
C_3	0.5

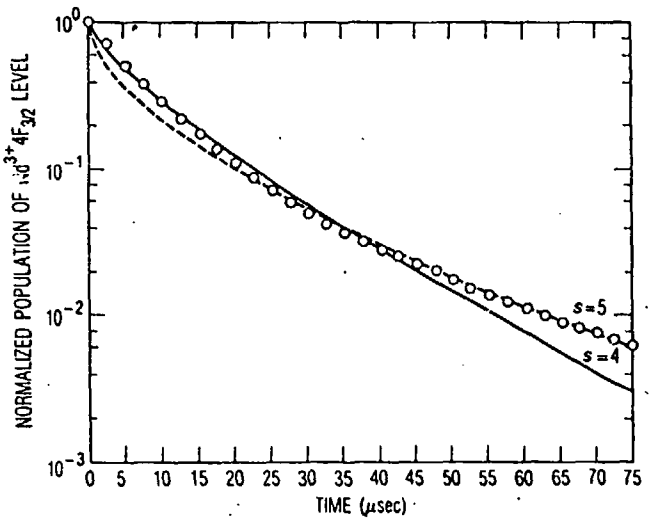

Fig. 7. Decay functions of the $^4F_{3/2}$ Nd^{3+} ions calculated by using the energy transfer theory compared with the experimental data (circles).

able to derive an expression for the donor luminescence that is macroscopically measurable:

$$\phi(t) = \exp\left[-\frac{t}{\tau_0} - \Gamma\left(1-\frac{3}{s}\right)\frac{4}{3}\pi c_a R_0^3\left(\frac{t}{\tau_0}\right)^{3/s}\right], \quad (11)$$

where $\Gamma(x)$ is the gamma function and c_a is the concentration of acceptor ions (cm^{-3}). Equation (11) covers several important situations. Namely, s = 6, 8, 10 corresponds to electric dipole–dipole, dipole–quadrupole, and quadrupole–quadrupole interactions, respectively. Equation (11) has been used for analyzing our experiment. The least-squares fits of Eq. (11) to the experimental data, using the most commonly encountered three electric multipolar interaction mechanisms, i.e. s = 6, 8, 10, are plotted in Fig. 6.

As Fig. 6 shows, the best fit is obtained with s = 6, implying a dipole–dipole interaction as expected. However, a better fit is obtained with s = 4 for the initial decay and s = 5 for the subsequent decay. The results are presented in Fig. 7. It is possible that this behavior is a result of the situation in which two or more Er^{3+} ions interact with one Nd^{3+} ion.

The corresponding critical transfer distance R_0 is 7.39 Å for s = 4 and 7.87 Å for s = 5. The interaction strength α, defined as $\alpha = R_0^s/\tau_0$, is 1.26×10^{-25} cm^4/sec for s = 4 and 1.27×10^{-32} cm^5/sec for s = 5.

DISCUSSION

As Fig. 1(a) shows, the fluorescence decay of the Er^{3+} $^4I_{11/2}$ state in Er:YAG is nonexponential. This is due mainly to the cross relaxation of the Er^{3+} ions in the $^4I_{13/2}$ state,[7] which is significant only in high-concentration Er^{3+}-doped materials. This process has been shown[7,17] to be responsible for the quasi-cw lasing at ~3 μm from the Er-doped laser crytals. On the other hand, when Nd^{3+} ions are codoped into Er:YAG lattices, the decay of the Er^{3+} $^4I_{11/2}$ state is exponential, and the decay rate becomes twice as fast as in Er:YAG [Fig. 1(b)]. This is, as the investigation in the previous section showed, a result of the two cross-relaxation processes governed by C_1 and C_2. The process C_2 accelerates the relaxation of the Er^{3+} $^4I_{13/2}$ state so that the Er population reservoir in this state is, to a large extent, eliminated. As a result, the cross-relaxation process from this state is prevented from taking place because the cross-relaxation rate is proportional to the number density of the ions in this state. Moreover, the internal pumping process for the Er^{3+} $^4I_{11/2}$ offered by this cross relaxation is disabled, which would otherwise pump the Er^{3+} $^4I_{11/2}$ state. The process C_1, on the other hand, simply opens up another channel for relaxing the Er^{3+} $^4I_{11/2}$ state in (Er, Nd):YAG in addition to the spontaneous and phonon-assisted emission from this state. Inevitably, this process results in a faster decay rate of the Er^{3+} $^4I_{11/2}$ state. In addition, because this process functions through nonradiative energy transfer, it removes some of the $^4I_{11/2}$ state Er^{3+} population that would otherwise have been available for stimulated emission. Clearly, both processes described by C_1 and C_2 militate against laser action by the Er^{3+} ions at 2.94 μm.

As far as the decay of excited Nd^{3+} ions is concerned, the calculations in the previous section revealed that this decay is governed predominantly by the dipole–dipole interactions between the excited-state Nd^{3+} ions ($^4F_{3/2}$) and ground-state Er^{3+} ions ($^4I_{15/2}$). The best fit between calculation and experimental data with s = 4 and s = 5 in the inverse-power rate model represents a special situation of the dipole–dipole interaction, as pointed out by Inokuti and Hirayama.[14] As a matter of fact, the transfer rate $n(R)$ can take a different inverse power of R dependence, which can be either greater than or smaller than 6, depending on whether the effective transfer is of shorter or longer range, if the system under study contains effects that were excluded in the theory. Our result is just an example of this situation. Further study is needed to resolve the detailed physical processes that are involved.

Moreover, the interaction discussed above that occurs between Er^{3+} and Nd^{3+} ions is clearly detrimental to the laser action of Nd^{3+} at 1.06 μm because the nonradiative interaction removes the Nd^{3+} population in the $^4F_{3/2}$ state, which would otherwise be available for lasing action. Actually, we can calculate the relative luminescence yield of the $^4F_{3/2}$ Nd^{3+} ions from[14]

$$\eta/\eta_0 = \frac{1}{\tau_0}\int_0^\infty \phi(t)dt, \tag{12}$$

where η_0 is the luminescence yield of the $^4F_{3/2}$ Nd^{3+} ions when Er^{3+} ions are not present and is equal to unity. Numerical evaluation of Eq. (12) gives $\eta/\eta_0 = 3.84\%$. This number matches the 30-times reduction in the lifetime of the $^4F_{3/2}$ Nd^{3+} ions in (Er, Nd):YAG as compared with Nd:YAG.

The above analysis helps us to understand the observation of relatively higher-input energy thresholds and lower efficiencies of the laser action from (Er, Nd):YAG at both 1.06 and 2.94 μm; this observation was made in our early studies of this laser material.[3]

In conclusion, the unusual fluorescence decay properties of the (Er, Nd):YAG crystal were explained by unlike ion–ion cross-relaxation mechanisms and energy transfer theory. The lasing performance of this material, as studied earlier elsewhere, is also understandable on the basis of these models. Complete elimination of self-termination in the Er^{3+} 2.94-μm transition has not been accomplished [namely, $\tau(Er^{3+}\,{}^4I_{13/2})$ is still longer than $\tau(Er^{3+}\,{}^4I_{11/2})$] in (15% Er, 1% Nd):YAG. However, we believe that this bottleneck should be unblocked by means of the combination of Er^{3+} and Nd^{3+} ions in crystals other than YAG in which the Er^{3+} ions have the shortest $^4I_{11/2}$ lifetime (~100 μsec). In the next phase of the study of this new class of multiple-wavelength solid-state lasers, hosts with longer Er^{3+} $^4I_{11/2}$ lifetimes will be sought.

ACKNOWLEDGMENTS

This research was supported by the U.S. Air Force Office of Scientific Research under contract AFOSR-84-0378. We are grateful to J. Machan for his assistance in some of the data acquisition work and to L. Zhu, who typed the manuscript of this paper.

* Current address, Departments of Electrical Engineering and Physics, Center for Research on Electro-Optics and Lasers, University of Central Florida, Orlando, Florida 32816-0001.

REFERENCES

1. Kh. S. Bogdasarov, V. I. Zhekov, V. A. Lobachev, T. M. Murina, and A. M. Prokhorov, "Steady-state emission from a $Y_3Al_5O_{12}$:Er^{3+} laser (λ = 2.94 μ, T = 300°K)," Sov. J. Quantum Electron. 13, 262 (1983).
2. M. Bass, W. Q. Shi, R. Kurtz, M. Kokta, and H. Diegl, "Operation of the high dopant density Er:YAG at 2.94 μm," in *Tunable Solid State Lasers II*, A. B. Budgor, L. Esterowitz, and L. G. DeShazer, eds., Vol. 52 of Springer Series in Optical Solid Sciences (Springer-Verlag, Berlin, 1986), pp. 300–305.
3. W. Q. Shi, R. Kurtz, J. Machan, M. Bass, M. Birnbaum, and M. Kokta, "Simultaneous, multiple wavelength lasing of (Er, Nd):$Y_3Al_5O_{12}$," Appl. Phys. Lett. 51, 1218 (1987).
4. A. A. Kaminskii, T. I. Butaeva, A. O. Ivanov, I. V. Mochalov, A. G. Petrosyan, G. I. Rogov, and V. A. Fedorov, "New data on stimulated emission of crystals containing Er^{3+} and Ho^{3+} ions," Sov. Tech. Phys. Lett. 2, 308 (1976).
5. A. A. Kaminskii, *Laser Crystals* (Springer-Verlag, Berlin, 1981).
6. V. I. Zhekov, T. M. Murina, A. M. Prokhorov, M. I. Studenikin, S. Georgescu, V. Lupei, and I. Ursu, "Cooperative process in $Y_3Al_5O_{12}$:Er^{3+} crystals," Sov. J. Quantum Electron. 16, 274 (1986).
7. W. Q. Shi, M. Bass, and M. Birnbaum, "Effects of energy transfer amongst Er^{3+} ions on the fluorescence decay and lasing properties of heavily doped Er:$Y_3Al_5O_{12}$," submitted to J. Opt. Soc. Am. B.
8. E. V. Zharikov, V. I. Zhekov, T. M. Murina, V. V. Osiko, M. I. Timoshechkin, and I. A. Shcherbakov, "Cross section of the $^4I_{11/2}$–$^4I_{13/2}$ laser transition in Er^{3+} ions in yttrium–erbium–aluminum garnet cyrstals," Sov. J. Quantum Electron. 7, 117 (1977).
9. See, for example, C. E. Pearson, *Numerical Method in Engineering and Science* (Van Nostrand Reinhold, New York, 1986).
10. S. Georgescu, V. Lupei, I. Ursu, V. I. Zhekov, V. A. Lobachev, T. M. Murina, and A. M. Prokhorov, "The role of the cross-relaxation mechanisms in the quasistationary generation regime of the YAG:Er laser," presented at the Second International Conference on Trends in Quantum Electronics, Bucharest, Romania, September 1985.
11. W. Koechner, *Solid-State Laser Engineering*, Vol. 1 of Springer Series in Optical Sciences (Springer-Verlag, Berlin, 1976).
12. G. M. Zverev, G. Ya. Kolodnyi, and A. M. Onishchenko, "Nonradiative transitions between levels of trivalent rare-earth ions in yttrium-aluminum garnet crystals," Sov. Phys. JETP 33, 497 (1971).
13. R. K. Watts and H. J. Richter, "Diffusion and transfer of optical excitation in YF_3:Yb,Ho," Phys. Rev. B 6, 1584 (1972).
14. M. Inokuti and F. Hirayama, "Influence of energy transfers by the exchange mechanism on donor luminescence," J. Chem. Phys. 43, 1978 (1965).
15. Th. Förster, "Zwischenmolekulare Energiewanderung und Fluoreszenz," Ann. Phys. (Leipzig) 2, 55 (1984); "Experimentelle und theoretische untersuchung des zwischenmolekularen Übergangs von Elektronenanregungsenergie," Z. Naturforsch. A4, 321 (1949).
16. D. L. Dexter, "A theoryof sensitized luminescence in solids," J. Chem. Phys. 21, 836 (1953).
17. V. I. Zhekov, V. A. Lobachev, T. M. Murina, and A. M. Prokhorov, "Cooperative phenomena in yttrium erbium aluminum garnet crystals," Sov. J. Quantum Electron. 14, 128 (1984).

Effects of Energy Transfer Amongst Er^{3+} Ions on the Fluorescence Decay and Lasing Properties of Heavily Doped $Er:Y_3Al_5O_{12}$

W. Q. Shi, M. Bass[*] *and M. Birnbaum*

Center for Laser Studies

University of Southern California

Los Angeles, CA 90089-1112

May 12, 1988

[*]Center for Research on Electro Optics and Lasers, University of Central Florida, Orlando, FL 32816-0001.

Abstract

Non-exponential fluorescence decay has been observed from both $^4I_{11/2}$ and $^4I_{13/2}$ states of Er^{3+} ions in heavily doped Er:YAG at room temperature. Processes of cross relaxation originating on these states are shown to be responsible. Rate equations including cross relaxation processes are written and numerically solved to result in the determination of the cross relaxation coefficients. It is found that these coefficients do not change with Er^{3+} concentration as opposed to that which has been reported previously by other workers. In addition, calculations of the Er^{3+} $^4I_{13/2}$ state decay functions are carried out using the energy transfer theory based upon the inverse-power-rate model. In the course of these calculations, energy migration between the $^4I_{13/2}$ state Er^{3+} ions was assumed to be very fast compared with the direct donor-acceptor energy transfer and the time scale of our measurement. As a result, all of the $^4I_{13/2}$ Er^{3+} sites were treated as equivalent and the transfer rate observed was considered to be simply that of the donor-acceptor pair transfer. These analyses indicated that the experimental data were consistent with a dipole-dipole interaction mechanism between the donor and acceptor ions. The impact of energy transfer between Er^{3+} ions on fluorescence decay and lasing properties is discussed.

Introduction

Since 2.94 μm laser action in high concentration ($\geq$ 10% Er^{3+}) Er:YAG was reported by Zharikov *et al* in 1975,[1] researchers have attempted to improve the lasing properties of this crystal and to understand the physics of the system. The 2.94 μm lasing transition in Er:YAG occurs between the $^4I_{11/2}$ and the $^4I_{13/2}$ states of the Er^{3+} ions. Unlike most four-level lasers, the lifetime of the upper lasing level ($^4I_{11/2}$) of the Er^{+3} ions in YAG is shorter than that of the lower one ($^4I_{13/2}$), making the 2.94 μm lasing transition self terminate. That is, as lasing proceeds, population in $^4I_{13/2}$ level accumulates due to stimulated emission and does not relax rapidly enough to maintain the required population inversion. Despite this bottleneck, quasi-continuous lasing at 2.94 μm has been observed from Er:YAG in long pulse operation,[2][3] suggesting the existence of additional processes which counteract the tendency for lasing to self terminate.

Recently, Zhekov *et al*[8] studied fluorescence decay properties of high concentration Er:YAG. They observed non-exponential behavior of the decay from the Er $^4I_{11/2}$ state when the sample was excited by intense pump pulses. They also noticed that fluorescence kinetics of the $^4I_{11/2}$ and $^4I_{13/2}$ in Er:YAG could be described by a simple exponential only under weak pump conditions. The non-exponential decay of highly doped Er:YAG was attributed to the cross relaxation of Er^{3+} ions excited to the $^4I_{11/2}$ and $^4I_{13/2}$ states in YAG.

An examination of the energy levels of Er:YAG [4] reveal that at room temperature energy resonances exist between several pairs of energy levels so that Er^{3+} ions in these states can cross relax in different ways shown in Fig. 1. In Er:YAG, the $^2H_{11/2}$ and $^4S_{3/2}$ states are very close to each other. They are among the levels into which ground state ions are excited by external pumping sources such as flashlamps.[5] The relaxation of excited ions in these two states involves three different mechanisms: radiative transitions, multiphonon transitions and cross relaxation. Fluorescence kinetics studies have shown that cross relaxation processes in heavily doped Er:YAG play a dominant role in relaxing the $^4S_{3/2}$ state at room temperature.[6] These processes populate

the $^4I_{11/2}$ and $^4I_{13/2}$ states equally and are governed by the coefficient W as shown in Fig. 1.[7] Even so, a population inversion is possible between the second Stark level of the $^4I_{11/2}$ state and the seventh Stark level of the $^4I_{13/2}$ due to the thermal distribution of populations in these manifolds at room temperature. This gives rise to lasing at 2.94 μm.

Also shown in Fig. 1 are cross relaxation processes governed by the coefficients W_1 and W_2 which originate in the $^4I_{13/2}$ and $^4I_{11/2}$ states, respectively. Cross relaxation of the $^4I_{13/2}$ level of Er^{3+} ions involves decay of one ion from this level to the ground state ($^4I_{15/2}$) and simultaneous excitation of a second ion from the $^4I_{13/2}$ to the $^4I_{9/2}$. The ion in the $^4I_{9/2}$ state rapidly relaxes to the $^4I_{11/2}$ so that the net change in the population inversion is +3. Cross relaxation of the $^4I_{11/2}$ state of Er^{3+} ions involves decay of one ion from the $^4I_{11/2}$ to the $^4I_{15/2}$ ground state and simultaneous excitation of another ion from the $^4I_{11/2}$ to the $^4S_{3/2}$ level. The ion in the $^4S_{3/2}$ level has an equal probability to decay to the $^4I_{11/2}$ or to the $^4I_{13/2}$ level. These processes result in a net change of -2 in the population inversion between the $^4I_{11/2}$ and $^4I_{13/2}$ levels. As will be discussed in the remainder of this paper, the two cross relaxation processes play major roles in determining the fluorescence and lasing properties of Er:YAG. Accurate determination of both W_1 and W_2 is important in order to describe Er:YAG in a quantitative manner and to design a laser for optimized performance.

It should be noted that for all of the cross relaxation processes discussed above, the transition probability equals the cross relaxation coefficient multiplied by the population of the state where the process originates.[2] Therefore, the cross relaxation rates change with time during pulsed lasing. In this paper, the values of W_1 and W_2 are determined for Er:YAG of different Er^{3+} concentrations by studying the observed fluorescence decay properties of both $^4I_{11/2}$ and $^4I_{13/2}$ levels in Er:YAG. This kind of study results in information that is useful in determining optimal Er concentration in laser design and in modelling laser dynamics as well. The results show that the cross relaxation coefficients W_1 and W_2 do not change with Er concentration, as opposed to

the square dependence(i.e. $W_1 \propto c^2$, where c = Er concentration) proposed by Zhekov *el al*[8]. The theory of energy transfer, based on the inverse-power-rate model, is also used to study the mechanisms of the energy transfer among Er^{3+} ions in the $^4I_{13/2}$ state. The influences of the cross relaxation processes on both fluorescence decay and lasing properties of heavily doped Er:YAG are discussed.

Experimental Observation of Fluorescence Decay from the Er^{3+} $^4I_{11/2}$ Level

The Er:YAG sample was excited with a Q-switched, frequency doubled Nd:YAG laser. The energy states studied were the $^4I_{11/2}$ and $^4I_{13/2}$. The transition lines monitored were $\sim$ 1.007 μm($^4I_{11/2} \longrightarrow {}^4I_{15/2}$) and $\sim$ 1.63 μm($^4I_{13/2} \longrightarrow {}^4I_{15/2}$). These fluorescence wavelengths were selected with a 0.27 m monochromator and the decay signals were detected by a liquid nitrogen cooled InSb infrared detector with a response time of $\leq$ 1 μsec. These decay signals were then recorded by a computer controlled data acquisition system for storage and processing. Each decay signal was stored and normalized so that the decay signal at any time represents the fractional population in the state on which the decay originates. The computer was programmed to average a selected number of decay signals and to plot the log of that average versus time. The experimental decay curves from the Er^{3+} $^4I_{11/2}$ and $^4I_{13/2}$ levels of 16.7 at%, 33.3 % and 50 at% Er:YAG are presented in Figs. 2 and 3.

If the fluorescence decay were governed by a single exponential process, then data presented in Figs. 2 and 3 would appear as straight lines. However, it is evident from Figs. 2 and 3 that the decay of both the $^4I_{11/2}$ and $^4I_{13/2}$ levels of Er^{3+} ions in heavily doped Er:YAG can not be described by a single exponential. In the following section, this non-exponential decay behavior is shown to result from interactions between Er^{3+} ions.

The peak pump power used to obtain the non-exponential decay data in Figs. 2 and 3 was about 2×10^5 W with a pump pulse duration of $\sim$ 20 nsec. The beam size on the sample was $\sim$ 3 mm in diameter and the beam was not tightly focused in order to avoid sample damage. The pump rate was 10 Hz. It was found that with much lower pump power(less by an order of magnitude), the fluorescence from both the $^4I_{11/2}$ and $^4I_{13/2}$ levels of Er^{3+} ions in Er:YAG could be accounted for by single exponential decay processes, indicative of the decay lifetimes of the Er^{3+} states. These exponential decay data are also illustrated in Figs. 2 and 3. The decay lifetimes of the $^4I_{11/2}$ and $^4I_{13/2}$ states of Er:YAG are listed in Table I.

Such a dependence of the decay behavior on the excitation level can be expected because the cross relaxation probability is directly proportional to the number of ions present in the particular state[2]. In the case of weak pumping, the number of ions excited to states from which cross relaxation originates is less. As a result cross relaxation is greatly reduced. In addition, it is worth pointing out that decay rates of the fluorescence from both the $^4I_{11/2}$ and the $^4I_{13/2}$ states of 1 at% Er:YAG were not affected by the excitation level. As might be expected, they were found to be governed by single exponentials.

Determination of the Cross Relaxation Coefficients

A rate equation analysis for the coupled state populations is used to study the population distribution in various Er^{3+} energy states of interest and to evaluate the cross relaxation coefficients W_1 and W_2. The Er energy levels under consideration are the $^4S_{3/2} + {}^2H_{11/2}$ (4), $^4F_{9/2}$ (3), $^4I_{11/2}$ (2), $^4I_{13/2}$ (1) and $^4I_{15/2}$ (0). The numbers in the parentheses are used to label the indicated states in the rate equation calculations.

Rate equations were written including cross relaxation processes, spontaneous emission, multiphonon transitions and external excitation. Stimulated emission is excluded. This set of equations was normalized with respect to the Er ion concentration, C, of the crystal employed in experiment

so that the initial conditions were $n_0(t=0) = 1$, and $n_i(t=0) = 0$ where i = 1, 2, 3, 4. The resulting equations for the 5 energy levels are as follows:

$$\frac{dn_0}{dt} = -W_{04}n_0 + \frac{n_1}{\tau_1} - (n_0W)n_4 + (CW_1)n_1^2 + (CW_2)n_2^2 \quad (1)$$

$$\frac{dn_1}{dt} = \frac{n_2}{\tau_2} - \frac{n_1}{\tau_1} + (n_0W)n_4 - (2CW_1)n_1^2 \quad (2)$$

$$\frac{dn_2}{dt} = \frac{n_3}{\tau_3} - \frac{n_2}{\tau_2} + (n_0W)n_4 + (CW_1)n_1^2 - (2CW_2)n_2^2 \quad (3)$$

$$\frac{dn_3}{dt} = W_{43}^{mp}n_4 - \frac{n_3}{\tau_3} \quad (4)$$

$$\frac{dn_4}{dt} = W_{04}n_0 - \frac{n_4}{\tau_4} + (CW_2)n_2^2 \quad (5)$$

where

C = Er concentration of the sample;

W_{04} = external excitation rate;

n_i = normalized population of the i^{th} state;

τ_i = decay lifetime of the i^{th} state;

W_{43}^{mp} = multiphonon transition rate from "4" to "3" = $\frac{1}{\tau_4} - n_0W - \frac{1}{\tau_4^{rad}}$;

τ_4^{rad} = radiative lifetime of the $^4S_{3/2}$ level;

n_4W = cross relaxation rate of the $^4S_{3/2}$ level.

Several assumptions have been made in writing these equations. They are:

(1) $A_{4j} \ll W_{43}^{mp}$ and n_0W, therefore is neglected;

(2) $A_{3j} \ll W_{32}^{mp}$, therefore is neglected;

(3) $A_{20} \ll W_{21}^{mp}$ and W_2, therefore is neglected(note: $\eta_{qe}(Er^{3+}\ ^4I_{11/2})$ is less than 1.5%[9]).

where A_{ij} = radiative transition rate from the Er^{3+} state i to j, and W_{ij}^{mp} = multiphonon transition rate from the Er^{3+} state i to j.

Our goal was to evaluate W_1 and W_2, the only unknown parameters in the equations, by nu-

merically solving the set of coupled differential Eqs. $1 \sim 5$ and fitting the calculated decay functions with the observed ones. The numerical solutions of this set of rate equations were obtained by the Runge Kutta-Verner fifth and sixth order method.[10] The calculated population distributions of the $^4I_{13/2}$ and $^4I_{11/2}$ states (n_1 and n_2) as functions of time are the solid curves in Figs. 2 and 3. The parameters used for obtaining these results are listed in Tab. II. The values for W_1 and W_2 which give the best fits to the experimental fluorescence decay data of both the $^4I_{11/2}$ and $^4I_{13/2}$ states of Er:YAG are summarized in Table III, along with those published previously by other researchers. It was found in the course of the calculations that fitting of the experimental data was quite sensitive to the variance in values for W_1. For example, 20 % change in the values for W_1 may result in a noticeable deviation between the experimental decay curves and the calculated ones. On the other hand, however, the calculations were relatively insensitive to the change in W_2. As will be discussed in more detail later, this behavior was observed because the cross relaxation process represented by W_1 makes the dominant contribution to the non-exponential nature of the fluorescence decay of heavily doped Er:YAG.

Mechanisms of the Ion-Ion Interactions in Er:YAG

In this section, mechanisms of interactions between Er^{3+} ions are explored. The study is conducted by employing the theory of energy transfer within energy donor and acceptor pairs. As will be seen in the following section, interactions between Er^{3+} ions in the $^4I_{13/2}$ excited state, giving rise to the cross relaxation process represented by W_1 in Fig. 1, make a dominant contribution to the non-exponential nature of the fluorescence decay of both the $^4I_{11/2}$ and $^4I_{13/2}$ states and to the quasi-continuous lasing observed between these two states. Therefore, we concentrate our study on the interactions between Er^{3+} ions in the $^4I_{13/2}$ state.

Assume that the energy diffusion rate among interacting Er^{3+} ions in the $^4I_{13/2}$ state is much faster than the direct one-step donor-acceptor transfer rate and also much faster than the time

scale of the measurement. As a result, all $^4I_{13/2}$ Er^{3+} sites are equivalent and the experimentally observed transfer rate will be governed by that of the direct donor-acceptor transfer processes. This assumption can be justified by the fact that we dealing with energy transfer systems of high donor concentration. It has been shown by Watts and Richter[13], in their study of energy transfer mechaniams in (Yb, Ho):YF_3 crystals, that as the donor concentration was increased(to 20% for example), the energy diffusion among energy donor ions became stronger and stronger until the rapid diffusion effectively averaged the donor's environment of acceptors and the observed decay would be limited by the energy transfer between the nearest neighbor donor and acceptor ions. The assumption is also supported by the appropriate use of rate equation analysis in the previous section which was validated by the rapid diffusion among the Er^{3+} donor ions that removed the spatial inhomogeneities in the system[14].

Since we are studying a singly doped crystal, interactions occur between like ions, namely Er^{3+} ions. In this system, the role of energy donors is played by the $^4I_{13/2}$ Er^{3+} ions which at the end of the energy transfer process will relax down to the ground ($^4I_{15/2}$) state, and that of the energy acceptors is played by $^4I_{13/2}$ Er^{3+} ions which will be found in the $^4I_{9/2}$ state when the transfer is finished. The total rate of transfer from a donor ion to an acceptor ion at a distance R can be expressed as:

$$W_T(R) = \frac{1}{\tau_0} + n(R) \tag{6}$$

where τ_0 is the intrinsic lifetime of the donor ions and n(R) is the transfer rate of a pair of interacting ions that are a distance R apart away from each other. Using the inverse-power-rate model developed on the basis of the Förstor-Dexter theory[15] [16], in which the transfer rate n(R) is written as the inverse power of the distance R,

$$n(R) = \frac{1}{\tau_0}(\frac{R_0}{R})^s \tag{7}$$

Inokuti and Hirayama[17] derived an analytical expression for the donor luminescence as the fol-

lowing:

$$\phi(t) = exp(-\frac{t}{\tau_0} - C_s t^{\frac{3}{s}}) \tag{8}$$

where $C_s = \Gamma(1 - \frac{3}{s})\frac{4}{3}\pi c_a (R_0 \tau_0^{-\frac{1}{s}})^3$, and $\Gamma(x)$ is the gamma function, c_a is the concentration of acceptor ions in cm^{-3}, s is a positive number and R_0 is, according to Förstor[15], a critical distance such that the transfer rate n(R) equals the decay rate, τ_0^{-1}, of the donor when R is equal to R_0. Eq. (8) covers three important electric multipolar interaction mechanisms. Namely, electric dipole-dipole interaction for s = 6, dipole-quadrupole interaction for s = 8 and quadrupole-quadrupole interaction for s = 10, respectively. The least-square fits of Eq. (8) to the experimental decay curves of the Er^{3+} $^4I_{13/2}$ state of various Er concentrations were performed for all of the three interaction schemes. It has been found that decay data of all the samples studied could be resonably fitted by Eq. (8). Fig. 4 illustrates the result for the 16.7% Er:YAG. The values for C_s that represent the best fits to the dipole-dipole mechanism (s=6) are summarized in Table IV, along with some other parameters which will be discussed in the next section.

In the follcwing, we will evaluate the number density, c_a, of the a :ceptor Er^{3+} ions in the $^4I_{13/2}$ state that take part in energy transfer. This in turn allows us to calculate the critical distance R_0. We will treat the energy transfer as if governed by the dipole-dipole scheme, i.e. s = 6.

The relative luminescence yield of the Er^3 $^4I_{13/2}$ state can be calculated by the following[17]:

$$\eta/\eta_0 = \frac{1}{\tau_0}\int_0^\infty \phi(t)dt \tag{9}$$

where η_0 is the luminescence yield of the $^4I_{13/2}$ state when there is no energy transfer between Er^{3+} ions. Therefore

$$\frac{c_a + c_d}{c_t} = 1 - \eta/\eta_0 = 1 - \frac{\int_0^\infty \phi(t)dt}{\tau_0} \tag{10}$$

where $c_a(c_d)$ = number density of the acceptor(donor) ions and c_t = total number density of the $^4I_{13/2}$ state. Since energy transfer occurs in donor-acceptor ion pairs, $c_a = c_d$. As a result, we find

$$c_a = \frac{1}{2}c_t(1 - \frac{\int_0^\infty \phi(t)dt}{\tau_0}) \tag{11}$$

The numerical values for c_t obtained in the rate equation analysis and and those for the integral in Eq. (12) are listed in Table IV. The critical distance R_0, as defined in Eq. (8), are therefore obtained and also presented in Table IV. As Table IV shows, R_0 for 16.7% Er:YAG (36$\AA$) is greater than that for 50% Er:YAG (25$\AA$). This should not be considered as an indication that Er^{3+} ions interact more strongly in 16.7% Er:YAG than in 50% Er:YAG. Rather, it is because the decay rate of 16.7% Er:YAG is smaller than that of the 50% Er:YAG.

Discussion

Table I shows the decay lifetimes for the $^4I_{11/2}$ and $^4I_{13/2}$ states of Er:YAG of various doping levels. As can be seen in Table I, the $^4I_{11/2}$ state lifetimes do not vary with Er concentration, indicating that this level does not suffer from concentration quenching. For the $^4I_{13/2}$ level, on the other hand, the lifetime is about 8.5 msec for the 1% Er:AG, reaches 13.7 msec at 16.7% Er:YAG and then falls off. These behaviors agree with the observation of Zhekov *et al*[8]. When these lifetimes were measured, we noticed that in the case of 1% Er:YAG, the decay from both Er^{3+} $^4I_{11/2}$ and $^4I_{13/2}$ states could be always described by a single exponential function and was not affected by the excitation level. This was observed because the interaction between Er^{3+} ions are very weak due to the small Er concentration.

Consider the decay of population of Er^{3+} ions in the $^4I_{11/2}$ state (n_2) which is affected by both cross relaxation processes represented by W_1 and W_2. Neglecting the pumping term, the decay equation of the population n_2 is given as the following:

$$
\begin{aligned}
\frac{dn_2}{dt} &= -\frac{n_2}{\tau_2} + (CW_1)n_1^2 - (2CW_2)n_2^2 \\
&= -\frac{n_2}{\tau_2}[1 - \frac{(CW_1)n_1^2}{\frac{n_2}{\tau_2}} + \frac{(2CW_2)n_2^2}{\frac{n_2}{\tau_2}}] \\
&= -\frac{n_2}{\tau_2}[1 - d_1(t) + d_2(t)] \\
&= -\frac{n_2}{\tau_2}[1 + D(t)] \\
&= -\frac{n_2}{(\frac{\tau_2}{1+D(t)})} \qquad (12)
\end{aligned}
$$

where $d_1(t) = \frac{(CW_1)n_1^2}{\frac{n_2}{\tau_2}}$, $d_2 = \frac{(2CW_2)n_2^2}{\frac{n_2}{\tau_2}}$ and $D(t) = d_2(t) - d_1(t)$.

An examination of Eq. 9 reveals that $d_1(t)$ and $d_2(t)$ represent the relative effects of W_1 and W_2 respectively on the decay rate of Er^{3+} ions in the $^4I_{11/2}$ state with respect to the natural radiative and non-radiative multiphonon decay processes expressed by τ_2. The calculated values of $d_1(t)$, $d_2(t)$ and $D(t)$ as functions of time obtained from the earlier rate equation analyses in the preceding section are plotted in Fig. 5. for 50% Er:YAG.

As seen from Fig. 5, $d_2(t)$ is greater than $d_1(t)$ at early times so that $D(t)$ is positive. During such times the decay of the $^4I_{11/2}$ state (n_2) is accelerated because of the cross relaxation process represented by W_2. This process is actually detrimental to lasing action at 2.94 μm because it prevents the population inversion from developing. However, as the decay continues, the effect of W_2 becomes smaller and smaller than that of the W_1. This is so because the number of Er^{3+} ions in the $^4I_{11/2}$ state decreases with time due to fluorescence decay while the population of the $^4I_{13/2}$ state is still being built up. In other words, the decay rate of the $^4I_{11/2}$ state population is slowed down at later times because the accumulation of Er^{3+} ions in the lower lasing level($^4I_{13/2}$) adds to the population of the $^4I_{11/2}$ state by the cross relaxation process represented by W_1. The result of this cross relaxation is to continue to pump the $^4I_{11/2}$ state (refer to Fig. 1) even though the external excitation is over. Such a process is clearly beneficial to 2.94 μm lasing in that it offers an internal channel for maintaining the population inversion for a long period. D(t) plotted in Fig. 5

shows the trend of the overall decay of the population in the $^4I_{11/2}$ level due to the cross relaxation processes.

As far as stimulated emission is concerned, both the start and end times of lasing will be affected by the processes represented by W_1 and W_2. However, the end time is determined mainly by W_1. The $^4I_{11/2}$ and $^4I_{13/2}$ levels start with equal population because of the cross relaxation processes represented by W (see Fig. 1). The populations in the $^4I_{11/2}$ and $^4I_{13/2}$ levels distribute among the Stark sublevels according to the Boltzmann law and makes a population inversion possible. The influence of W_2 on the $^4I_{11/2}$ level will delay the formation of the population inversion. As pumping proceeds, W_1 becomes strong enough to balance out W_2 and the population inversion becomes large enough to result in net gain and lasing at 2.94 μm. This is why the 2.94 μm lasing reaches threshold after the peak of the pump[3]. Both W_1 and W_2 play a role in the initial stage of the laser emission of Er:YAG. On the other hand, as Fig. 5 shows, once D(t) becomes negative, it decreases monotonically. All this means is that the self-pumping process (W_1) keeps bringing Er ions from the $^4I_{13/2}$ to the $^4I_{11/2}$ level and helps maintain the population inversion even after the external pump pulse has ended. The quasi-continuous lasing operation observed at 2.94 μm can be understood.

Table III shows the cross relaxation coefficients W_1 and W_2 obtained in this work and reported previously by other researchers. Zhekov *et al* [8] [12] have previously measured the cross relaxation coefficients and found that, based on their results for 10%, 15% and 50% Er:YAG, the cross relaxation coefficient W_1 was proportional to the square of the Er concentration. However, as can be seen in Table III, the results of our measurements show that these coefficients are independent of the Er concentration. As a metter of fact, the values for W_1 of 10% and 15% Er:YAG determined by Zhekov *et al* are the same within the accuracy of their measurement(50%) and are consistent with those obtained by us. The exception seen for the 33.3% Er:YAG may be related to material purity considerations.

Under high excitation, decay of the Er^{3+} $^4I_{13/2}$ level is faster in the initial stage and gradually becomes slower and approaches the decay rate(Fig. 3). This occurs because the initial $^4I_{13/2}$ state population is large under the δ-function excitation and therefore the cross relaxation process W_1 is very efficient in removing population from the $^4I_{13/2}$ state, resulting in a faster initial decay. As decay continues, the state becomes less and less populated due to cross relaxation processes and fluorescence emission until the rate of cross relaxation of Er^{3+} ions in this state becomes negligible and the observed decay approaches its rate of the simple exponential decay observed only at low excitation level.

It has been found in the previous section that the $^4I_{13/2}$ state decay data were consistent with the dipole-dipole interaction mechanism. However, as seen in Fig. 4, good agreenment between the decay data and the dipole-quadrupole and quadrupole-quadrupole mechanisms were also obtained. In other words, these $^4I_{13/2}$ state decay data are not sensitively dependent upon the interaction mechanisms involved in the the energy transfer processes. This observation prevented us from unambiguously concluding that the dipole-dipole mechanism made the dominant contribution to the interactions among the $^4I_{13/2}$ state Er^{3+} ions in Er:YAG.

Conclusion

The cross relaxation coefficients of Er^{3+} ions in the $^4I_{11/2}$ and $^4I_{13/2}$ states, W_1 and W_2, have been determined by rate equation calculations. The results give evidence that these coefficients do not depend on Er^{3+} concentration. Only the cross relaxation transition rates are concentration dependent. The non-exponential decay of Er^{3+} $^4I_{11/2}$ fluorescence and the quasi-continuous lasing properties of heavily doped Er:YAG can be explained by proper understanding of the cross relaxation processes.

Energy transfer theory has been employed to study the mechanisms of the non-exponential decay of the Er^{3+} $^4I_{13/2}$ state. However, due to the insensitivy of our data to the interaction

mechanisms involved, we could not attribute the interaction between Er^{3+} ions to any particular electric multipolar interaction scheme at this moment. Further study on this issue is necessary before arriving at an definitive conclusion.

This work was supported by the Air Force Office of Scientific Research under contract No. AFOSR-84-0378. The authors are grateful to J. Machan who assisted in the data acquisition and processing tasks.

References

[1] E. V. Zharikov, V. I. Zhekov, L. A. Kulevskii, T. M. Murina, V. V. Osiko, A. M. Prokhorov, A. D. Savel'ev, V. V. Smirnov, B. P. Starikov and M. I. Timoshechkin, "Stimulated Emission from Er^{3+} Ions in Yttrium Aluminum Garnet Crystals at $\lambda = 2.94\ \mu$", *Sov. J. of Quantum Electronics 4, 1039 (1975)*

[2] Kh. S. Bagdasarov, V. I. Zhekov, V. A. Lobachev, T. M. Murina, and A. M. Prokhorov, "Steady-State Emission from a $Y_3Al_5O_{12}$:Er Laser ($\lambda = 2.94\ \mu$, T = 300°K), *Sov. J. of Quantum Electronics 13, 262 (1983)*

[3] M. Bass, W. Q. Shi, R. Kurtz, M. Kokta and H. Diegl, "Operation of The High Dopant Density Er:YAG at 2.94 μm", in *"Tunable Solid State Lasers II", eds. A. B. Budgor, L. Esterowitz and L. G. DeShazer, Springer Series in Optical Sciences 52, pp300-305 (Springer Verlag, Berlin 1986)*

[4] A. A. Kaminskii, *Laser Crystals (Springer-Verlag, Berlin 1981)*

[5] Kh. S. Bagdasarov, V. I. Zhekov, V. A. Lobachev, A. A. Manenkov, T. M. Murina and A. M. Prokhorov, "Cross Relaxation of a Laser Based on Yttrium-Aluminum Garnet with Er^{3+}", *Izvestiya Akademii Nauk SSSR. Seriya Fizicheskaya, 48, 1765 (1984)*

[6] S. Georgescu, V. Lupei, I. Ursu, V. I. Zhekov, V. A. Lobachev, T. M. Murina, A. M. Prokhorov, "The Role of the Cross-Relaxation Mechaniams in the Quasistationary Generation Regime of the YAG:Er Laser", *Second International Conference on Trends in Quantum Electronics, Bucharest, Romania, Sept. 1985, Paper I.C.1.9.*

[7] V. I. Zhekov, B. V. Zubov, V. A. Lobachev, T. M. Murina, A. M. Prokhorov, and A. F .Shevel', "Mechanism of a Population Inversion Between the $^4I_{11/2}$ and $^4I_{13/2}$ Levels of the Er^{3+} Ions in $Y_3Al_5O_{12}$ Crystals", *Sov. J. of Quantum Electronics 10, 428 (1980)*

[8] V. I. Zhekov, T. M. Murina, A. M. Prokhorov, M. I. Studenikin, S. Georgescu, V. Lupei, and I. Ursu, "Cooperative Process in $Y_3Al_5O_{12}$:Er^{3+} Crystals", *Sov. J. of Quantum Electronics, 16 , 274 (1986)*

[9] E. V. Zharikov, V. I. Zhekov, T. M. Murina, V. V. Osiko, M. I. Timoshechkin, and I. A. Shcherbakov, "Cross Section of the $^4I_{11/2} - {}^4I_{13/2}$ Laser Transition in Er^{3+} Ions in Yttrium-Erbium-Aluminum Garnet Crystals", *Sov. J. of Quantum Electronics, 7, 117 (1977)*

[10] See for example: C. E. Pearson, "Numerical Method in Engineering and Science", *(Van Norstand Reinhold Company, Inc., New York 1986)*

[11] Our results

[12] V. I. Zhekov, V. A. Lobachev, T. M. Murina, and A. M. Prokhorov, "Cooperative Phenomena in Yttrium Erbium Aluminum Garnet Crystals", *Sov. J. of Quantum Electronics, 14, 128 (1984)*

[13] R. K. Watts and H. J. Richter, "Diffusion and Transfer of Optical Excitation in YF_3:Yb, Ho", *Phys. Rev., B6, 1584 (1972)*

[14] J. C. Wright, "Up-Conversion and Excited State Energy Transfer in Rare-Earth Doped Materials",

[15] Th. Förstor, "Zwischenmolekulare Energiewwanderung und Sluoreszenz", *Ann. Phys. (Leipzig), 2, 55 (1948)*; "Experimentelle und Theoretische Untersuchung Esdes Zwisccchenmolekularen Übeergangs von Elektronenanregungsenergie", *Z. Naturforsch. Tail A4, 321 (1949)*

[16] D. L. Dexter, "A Theory of Sensitized Luminescence in Solids", *J. of Chem. Phys., 21, 836, (1953)*

[17] M. Inokuti and F. Hirayama, "Influence of Energy Transfer by the Exchange Mechanism on Donor Luminescence", *J. of Chem. Phys.*, *43,1978 (1965)*

Table I. Intrinsic Decay Lifetimes of Er:$Y_3Al_5O_{12}$

Concentration	$^4I_{11/2}$ (μsec)	$^4I_{13/2}$(msec)
1 at%	102	8.56
16.7 at%	105	13.74
33.3 at%	94	9.58
40 at%	96	7.14
50 at%	93	4.19
60 at%	97	1.95

*All the values are good within $\pm$ 5%.

Table II. Parameters Used in Rate Equation Calculations

parameters	values	reference
C(16.7 at%)	2.32×10^{21} cm^{-3}	[11]
C(33.3 at%)	4.66×10^{21} cm^{-3}	[11]
C(50.0 at%)	7.00×10^{21} cm^{-3}	[11]
τ_1	see Table I	[11]
τ_2	see Table I	[11]
τ_3	1.2 μsec *	[8]
τ_4	1.0 μsec *	[8]
W_{43}^{mp}	1.8×10^5 sec^{-1} *	[6]
n_0W	9.3×10^5 sec^{-1} *	[6]

* These parameters were assumed to be the same for all concentration in the calculations.

Table III. Cross Relaxation Coefficients of Er:YAG

Concentration (%)	$W_1(cm^3 \cdot sec^{-1})$	$W_2(cm^3 \cdot sec^{-1})$	Reference
10	1.8×10^{-17}	5.1×10^{-17}	[8]
15	2.5×10^{-17}	—	[12]
16.6	1.5×10^{-17}	3.0×10^{-17}	[11]
33.3	4.0×10^{-17}	3.0×10^{-17}	[11]
50	2.5×10^{-17}	3.0×10^{-17}	[11]
	25.0×10^{-17}	—	[12]

Table IV. Ion-Ion Interaction Parameters in Er:YAG

Concentration	C_6 ($msec^{-\frac{3}{6}}$)	$c_t(\times 10^{19}\ cm^{-3})$	$\int_0^\infty \phi(t)dt$ (msec)	$c_a(\times 10^{18}\ cm^{-3})$	R_0 ($\mathring{A}$)
16.7	0.166	0.88	8.17	1.78	36
50	0.323	2.65	2.43	5.57	25

Figure Captions

Fig. 1 Energy level diagram for Er:YAG showing various radiative and non-radiative transitions and cross relaxation processes.

Fig. 2 Log of fluorescence strength versus time for the experimental (◯) and calculated(solid curve) decay functions of the Er^{3+} $^4I_{11/2}$ level of (a): 16.7% Er:YAG, (b): 33.3% Er:YAG and (c): 50% Er:YAG. All data are normalized to unity at t = 0. The calculated decay functions were obtained using a rate equation analysis.

Fig. 3 Log of fluorescence strength versus time for the experimental (◯) and calculated (solid curve) decay functions of the Er^{3+} $^4I_{13/2}$ level in 16.7%, 33.3% and 50% Er:YAG. All data are normalized to unity at t = 0. The calculated decay functions were obtained using a rate equation analysis.

Fig. 4 Log of fluorescence strength versus time for the experimental (◯) and calculated(solid curve) decay functions of the Er^{3+} $^4I_{13/2}$ level in 50% Er:YAG. The calculated decay functions were obtained using an energy transfer theory.

Fig. 5 Decay of the Er^{3+} $^4I_{11/2}$ level in the presence of cross relaxation processes.